FOURIER TRANSFORMED INFRARED PHOTOACOUSTIC SPECTROSCOPY OF SOLIDS

By

HUGH HILL RICHARDSON, JR.

Bachelor of Science

Oral Roberts University

Tulsa, Oklahoma

1979

Submitted to the faculty of the
Graduate College of the
Oklahoma State University
in partial fulfillment of
the requirements for
the Degree of
MASTER OF SCIENCE
May, 1982

FOURIER TRANSFORMED INFRARED

PHOTOACOUSTIC SPECTROSCOPY

OF SOLIDS

Thesis Approved:

M. G. Rockley

Thesis Advisor

J. Paul Devlin

Tom E. Moore

Norman N. Durham

Dean of Graduate College

TABLE OF CONTENTS

LIST OF TABLES

LIST OF FIGURES

CHAPTER I

HISTORICAL BACKGROUND

Photoacoustic spectroscopy had its beginning in 1880 when Alexander Graham Bell (1) presented his work on the photophone to the American Association for the Advancement of Science. He reported how he had accidentally discovered what is known today as the photoacoustic effect in solids. The apparatus that Bell used was very crude by today's standards - a voice-activated mirror, a selenium cell and an electrical telephone receiver. He chopped his light source (sunlight) by use of the voice-activated mirror, which was focused onto the selenium cell. The cell's electrical resistance varied with the intensity of the light. Bell discovered that he was able to obtain an audible signal by focusing the beam on a thin film of a solid which was sealed to a hearing tube. Further experimentation showed that if the solid was placed in a sealed chamber connected to the hearing tube, an audible signal was still obtained. Bell (1) observed that the loudest signals were obtained from porous materials and from materials with the darkest colors. He showed that the photoacoustic effect in solids was dependent upon the material absorbing the light, and that

the signal strength was proportional to the amount of light absorbed.

Bell and his associate, Sumner Tainter, branched out into the study of the photoacoustic effect in gases and liquids. They observed that of the two, gases were far superior in signal strength. From that point on, until recently, most of the work in photoacoustics was concerned with gases. Bell (2), Tyndall (3) and Roetgen (4) performed early experiments on gases in which they observed that audible signals were obtained from gases in sealed chambers. Colored gases absorbed visible light, while colorless gases absorbed infrared light. The audible signal was detected as pressure fluctuations having the same frequency as the chopping frequency. The acoustic pressure change was correctly attributed to the transformation of absorbed light into translational energy of the gas molecule. The technique surfaced again in 1938 when Viengerov (5) used it to study the effect of infrared light on gas mixture concentrations. He used a black body radiator (Nernst glow bar) as his infrared source. As a detector he used an electrostatic microphone which measured the voltage change between two charged capacitive diaphragms. With this technique he was able to measure CO_2 in N_2 gas of about .2% by volume. A year later Pfund (6) reported that instead of measuring pressure changes in the cell, a thermopile shielded from direct radiation could be used as a detector.

In 1943 Luft (7) showed that added sensitivity could be obtained (CO_2 in N_2 of ppm) if two photoacoustic cells were employed in a differential design. This was a precursor of an infrared gas spectrometer called the spectrophone (8).

In 1946 Gorelik (9) proposed that the phase of the photoacoustic signal could be used to determine the lifetime of the excited state for different gas molecules. This method relies on the principle that there is a time delay between the ground state absorption and the reemission of that energy by non-radiative processes. If there is a long delay between absorption of light and reemission of heat there will be a corresponding phase change with that of the chopped light. Thus, a study of the phase of the photoacoustic signal versus modulation frequency would lead to information about the lifetime of the excited state. In 1948 Slobodskaya (10) studied the vibrational lifetimes of gaseous molecules by this technique.

High brightness lasers have provided a new impetus for gas phase photoacoustic spectroscopy (PAS). Because the PA signal is linearly proportional to the strength of the incoming light, high brightness lasers have permitted the analysis of very low concentrations of gaseous mixtures (ppb) (11). M. B. Robins used this advantage to study the efficiencies of radiative and non-radiative channels of deexcitation for biacetyl. He was also able to study the intersystem crossing of gas mixtures of either pyridine or

oxygen with biacetyl (12) (13) (14) (15) (16).

Since 1973 the photoacoustic effect with solid samples has been studied by Rosencwaig (17). In the last few years the experiments performed indicate that the primary photoacoustic signal arises from periodic heat flow from the sample to the surrounding gas. The first attempt at a modern quantitative theory for photoacoustic spectroscopy for solids was made by Parker (18) in 1973. The problem with Parker's treatment was that it applied only to specific limiting cases and not to the general effect. Rosencwaig and Gersho (19) (20) proposed a more general theory for the photoacoustic effect on condensed media. This theory shows that the generation of the pressure fluctuation in the cell depends upon the acoustic pressure disturbance at the gas-sample interface and the propagation of this signal to the microphone. The acoustic pressure disturbance has been likened to a thermal piston moving as a function of the periodic heat flow from the sample to the gas. This thermal piston then causes an acoustical shock wave detected by the microphone. A particularly interesting special result arises from the general equation which applies to thermally thin, optically opaque samples. Carbon black is such a sample. In this particular case the signal is independent of the optical absorption coefficient but dependent upon the thermal properties of the backing material. The signal also varies as one over the modulation frequency. It is for this

reason that carbon black could be used as an excellent reference material. The photoacoustic spectrum of carbon black gives a characteristic spectrum for the spectrometer and photoacoustic cell (Fig. 1). A preliminary calculation shows that if the incident radiation is .8 milliwatts/cm^2, then the periodic pressure fluctuation is approximately .5 Newtons/m^2. This pressure change would produce a signal of 50 millivolts using a microphone having a sensitivity of 10 millivolts/microbar. Further additions to the photoacoustic theory were made by Bennett and Forman (21), Aamodt et al.

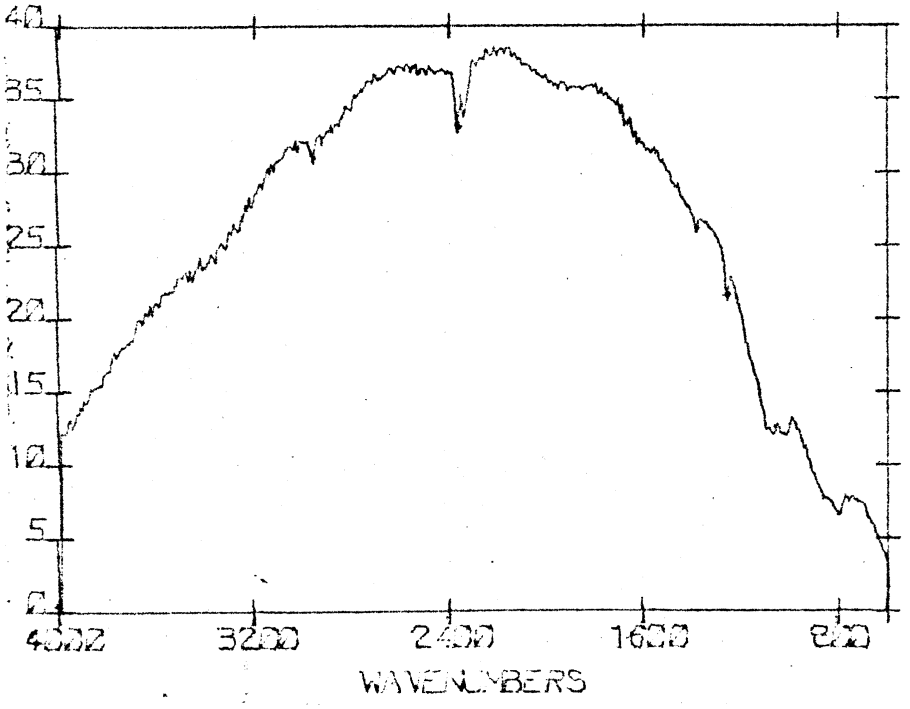

Figure 1. 20 Scans of Cotton Black at 8 cm^{-1} Resolution.

(22) and Wetsel and McDonald (23).

Most of the recent experimental work has been done with high power lasers (24). The disadvantage of this technique is that lasers can only scan over discrete wavelengths. Since the vibrational modes of compounds occur in the mid-IR region (4000 cm^{-1} to 600 cm^{-1}), it would be advantageous to develop a technique which could be used to study the photoacoustic effect in solids for this particular region of the electromagnetic spectrum. IR lasers can be used but a technique which involves a continuous source of radiaton offers the advantage of obtaining information over all wavelengths. The problem that plagued early attempts to obtain the photoacoustic spectrum of solids in the IR region was that the broadband infrared sources were too weak for using conventional monochromators. A method was developed by Farrow et al. (25) in 1978 which overcame this problem by adapting a Fourier Transformed Visible Spectrometer to do photoacoustics. This technique employs a Michelson interferometer, which has two main advantages over conventional monochromators. First, the data in an interferometer are collected from all spectral frequencies simultaneously throughout the measurement. This allows much higher signal/noise ratios than are obtainable from conventional monochromators. Second, an interferometer has a much higher optical throughput than a conventional monochromator. This concept has been carried into the mid-

IR region by Rockley (26). The development of this method and its exploitation are the subject of this thesis.

CHAPTER II

EXPERIMENTAL METHODS

With the implication of signal enhancement in mind, the experimental apparatus as well as the procedure used for the experimentation will be discussed here. Several important considerations relative to the study of the photoacoustic effect on solids will be addressed. The first consideration must be the sample cell used. Many criteria govern the actual design of the photoacoustic cell. The cell must be acoustically isolated from extraneous sources. Since in this study a Fourier Transformed Spectrometer was used instead of a lock-in amplifier, extraneous noise was a consideration. Acoustic room noise was the limiting noise factor (Fig. 2). The Fourier Transformed Spectrometer used modulated the beam between 1265-100 Hz. In order to reduce electronic noise, batteries were used to power the microphones. The cell was also placed on foam rubber supports to reduce interference from room vibrations. A second parameter that must be considered is minimization of extraneous signals within the cell itself. Optically transparent windows were used (NaCl or KBr). The cell was made either of polished aluminum or stainless steel in order

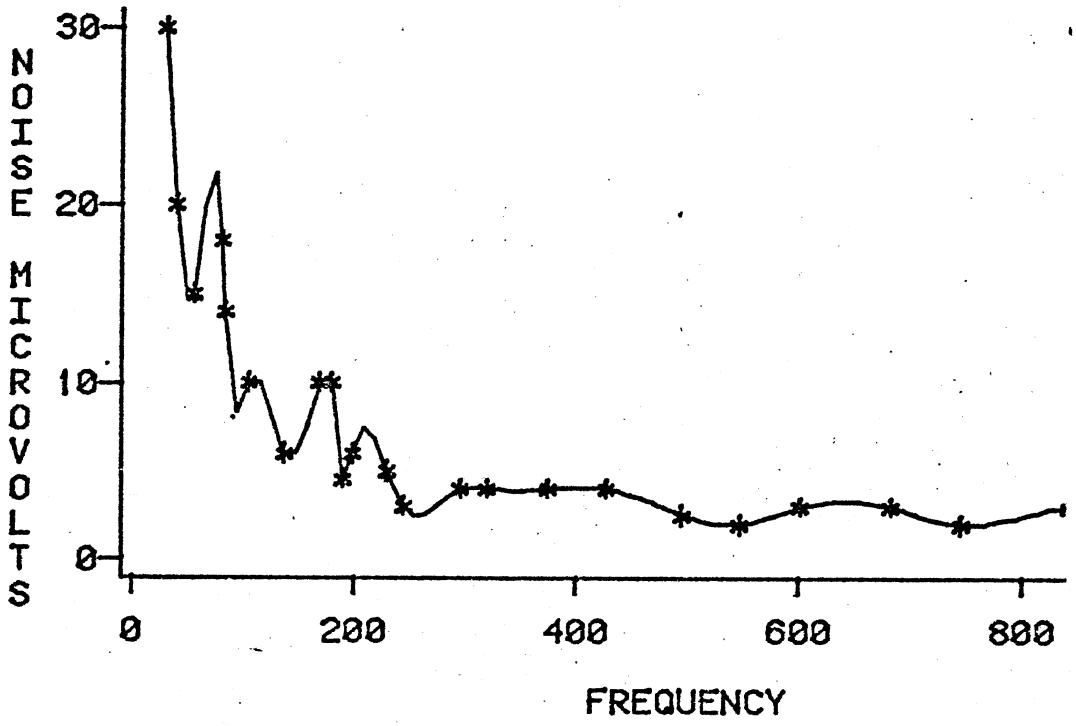

Figure 2. Noise from Cell with Respect to Modulation Frequency.

to reduce the magnitude of the signal from the cell material itself. The microphone used is also an important parameter and must have a flat frequency response over a wide acoustic range. The first microphone choice was a General Radio 1/2" diameter foil Electret Microphone (model 1962), which has a sensitivity of about 10 mv/microbar with a flat frequency response from 5-20,000 Hz. An Ithaco low-noise 40 dB preamplifier (model 143L) was used to amplify the microphone signal. All of the spectra discussed in this thesis were

measured with this microphone and preamplifier. However, recent research using a more sensitive microphone (50 millivolts/microbar) preamplifier assembly (Bruel Kjaer 1/2" foil electret microphone, model 4175, with a 2642 preamplifier and 2810 power supply) has shown that signal enhancement can be obtained with a sensitive microphone but a limit to the signal to noise ratio was reached at about 1% with 20 scans.

There are many different ways of maximizing the acoustic signal within the cell. Since the PA signal is inversely proportional to the cell gas volume, an attempt to minimize the gas volume should be made. However, as the gas volume is minimized, a point is reached where the signal suffers appreciable losses due to dissipation to the cell windows and walls before reaching the microphone. This point is approximately at the thermal diffusion length of the gas, which is inversely proportional to the square root of the modulation frequency. Considering the lowest chopping frequency (160 Hz) and air at room temperature and pressure, this would be about .015 cm. At high frequencies there is a competing effect known as the thermoviscous damping. The damping coefficient (E) is equal to

$$E = (N_e \, w \, / \, 2P_o)/d \, C_o$$

where d is the closest dimension between cell boundaries, C_o is the sound velocity, w is the frequency, P_o is the gas density and N_e is an effective viscosity. The exponential

attenuation should begin to damp the signal around 0.04 cm for 1600 Hz modulation frequency. For a particular cell used in the frequency range of 160-1600 Hz, the minimum distance between the sample and the window is around 1-2 mm.

Another choice for enhancing the acoustic signal is to construct a Helmholtz resonator from the cell (Fig. 3) (27).

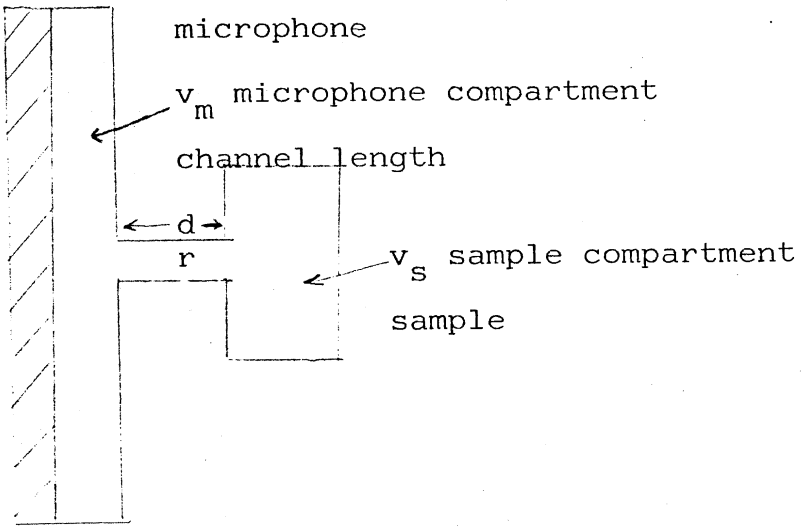

Figure 3. Helmholtz Resonator for PAS Showing Chamber Compartments.

The basic Helmholtz resonance frequency is given by

$$V_o = C_o \pi r^2 / 2 d V_e$$

where "r" is the channel radius, "d" is the channel length and "V_e" is $V_m V_s/(V_m + V_s)$. "V_m" is the microphone

department volume, and "V_s" is the sample department volume. The cells used for this work were natural Helmholtz resonators, but the Helmholtz resonance frequency was much higher than the experimental modulation frequency. For the greased cell (Fig. 4) the Helmholtz frequency would be 2055 Hz, which is above the modulation frequency at 4000 cm^{-1}.

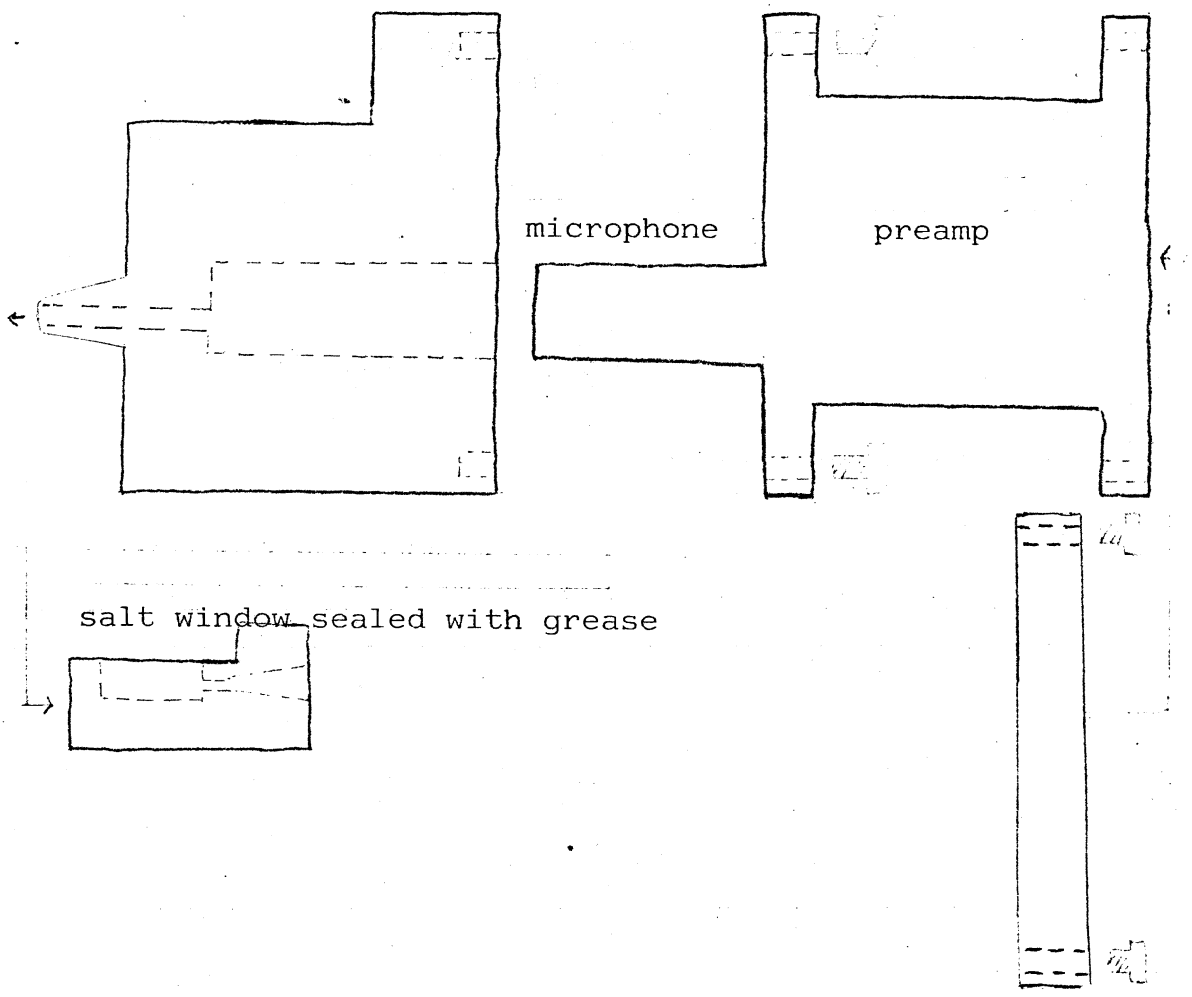

Figure 4. Greased Cell.

Therefore, it appeared that for the type of cells used, the Helmholtz advantage was well outside the experimental modulation frequency range. The minimum volume cell (Fig. 5) introduced a much higher Helmholtz resonance frequency. (Figures 4 and 5 are the acoustic cells that were used. Notice in Figure 4 that the greased cell contains microphone and preamplifier assembly all as one unit. For the minimum volume cell shown in Fig. 5, the microphone is housed inside

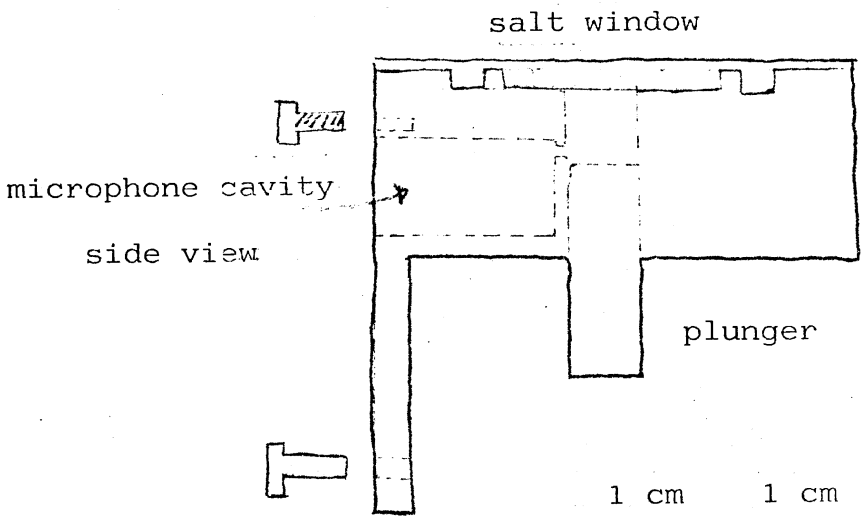

Figure 5. Minimun Volume Cell.

the cell, while the preamplifier and power supply are separate components.

Yet another method of increasing the photoacoustic

signal without further modification of the cell is to use gases with high thermal conductivity as well as high pressures and low temperatures. This method increases the photoacoustic signal, because the signal is proportional to ($K P_o / T_o$) where "K" is the thermal conductivity of the gas, "P_o" is the ambient pressure and "T_o" is the ambient temperature.

Experimental Procedure

Following is the experimental procedure used in most of the work discussed here. Most samples studied as powders were first finely ground with a mortar and pestle. A small aluminum pan was formed by shaping aluminum foil around the end of a small cylinder. This pan was used to hold the sample. The salt window was cleaned of all vacuum grease with Skelly B and polished until it was transparent. Grease was used (Fig. 4) to seal the window to the cell. Freshly activated molecular sieves were placed inside the cell chamber. An aluminum partition was placed on top of the sieves, and the sample was sealed in the chamber with the salt window. The microphone output was fed into the spectrometer by an adapter, allowing a transition from the conventional spectrometer to the photoacoustic apparatus without having to break the vacuum seal. The cell was placed in a prearranged location in the sample compartment, roughly optimizing the signal intensity with respect to the

6x condensing lens mirror assembly. An adjustment of cell position was made to maximize the interferrogram. The spectrum was then ratioed to a reference spectrum of carbon black to eliminate non-uniform signal intensity with respect to wavelength due to the black body radiator curve of the glow bar (Fig. 6), the optics and the cell parameters.

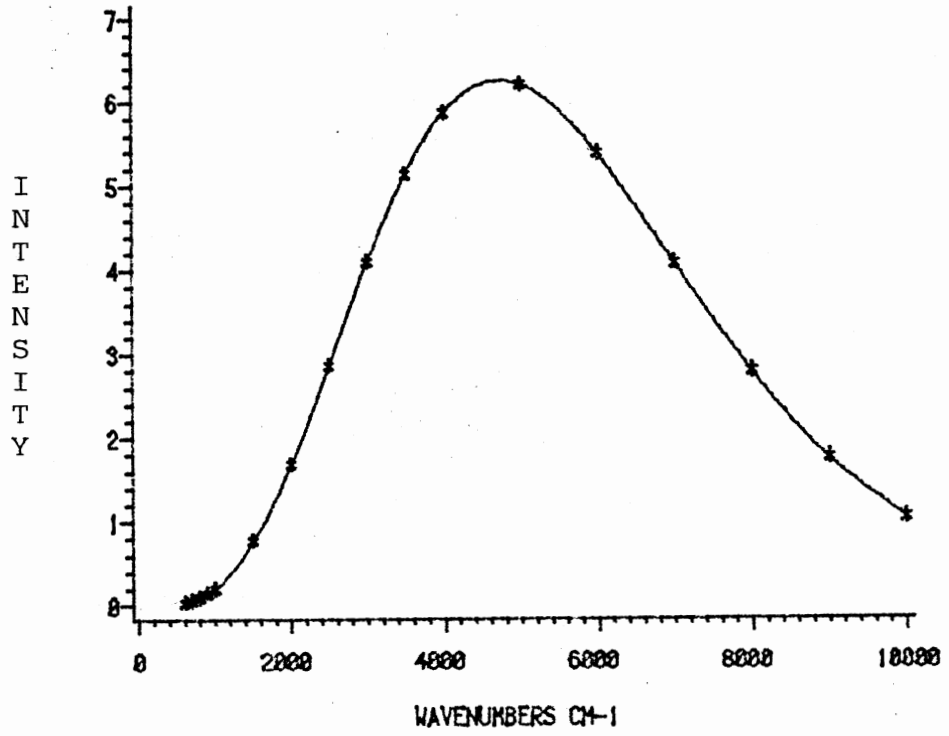

Figure 6. Black Body Curve for a Glowbar at 1100° C.

CHAPTER III

RESULTS AND CONCLUSIONS

Three main questions of interest emerge in studying the photoacoustic effect of solids in the infrared region using a Fourier Transformed Spectrometer. Could this technique produce good qualitative results? Could this technique produce good quantitative results? What factors affect the quality of the photoacoustic signal obtained? Experiments were designed to answer these questions.

The first set of experiments were intended to address the question of qualitative results. For this, three different types of solid samples were chosen: 1) a variety of biological materials of interest in body metabolism, 2) asbestos fibers playing a part in contamination of air and water supplies, and 3) biologically active drugs.

Biological Materials

The Fourier Transformed Infrared Photoacoustic Spectrum (FTIR-PAS) of protoporphyrin IX dimethyl (Fig. 7), hemin (Fig. 8) and hemoglobin (Fig. 9) and horseradish peroxidase (Fig. 10) were obtained to determine if this technique yielded qualitative information. The spectra are shown in

Figures 7-10.

The spectrum of protoporphyrin IX dimethyl ester (Fig. 7) is qualitatively identical to that reported by Boucher and Katz (28). The only quantitative difference is in the relative absorbance of the methyl propionate ester carbonyl stretch at 1738 cm^{-1} seen by the two methods. By comparison with the rest of the spectrum, the PAS signal strength for this band is much less than that reported by Boucher and Katz. With this exception, the remarkable agreement between the spectra obtained by the two methods show that FTIR-PAS is capable of yielding structural information on undiluted solid samples without the need for sample preparation.

The spectrum of hemin (Fig. 8) is remarkably similar to the conventional transmission spectrum (29). The sharp absorption due to the N-H stretch in protoporphyrin IX is absent in the spectrum of hemin, as expected. In hemin the nitrogens of the porphyrin ring structures are coordinately bonded to the iron in the center of the ring (Fig. 11).

The spectra of hemoglobin (Fig. 9) and horseradish peroxidase (Fig. 10) are similar. They show broad, almost structureless, absorption, again as might be expected. The wealth of different bonds found in the proteins attached to the central prophyrin structure crowd the spectra, with the result that little structural information can be inferred. They are, however, distinguishable. The important fact here is that both of these spectra were measured on samples that

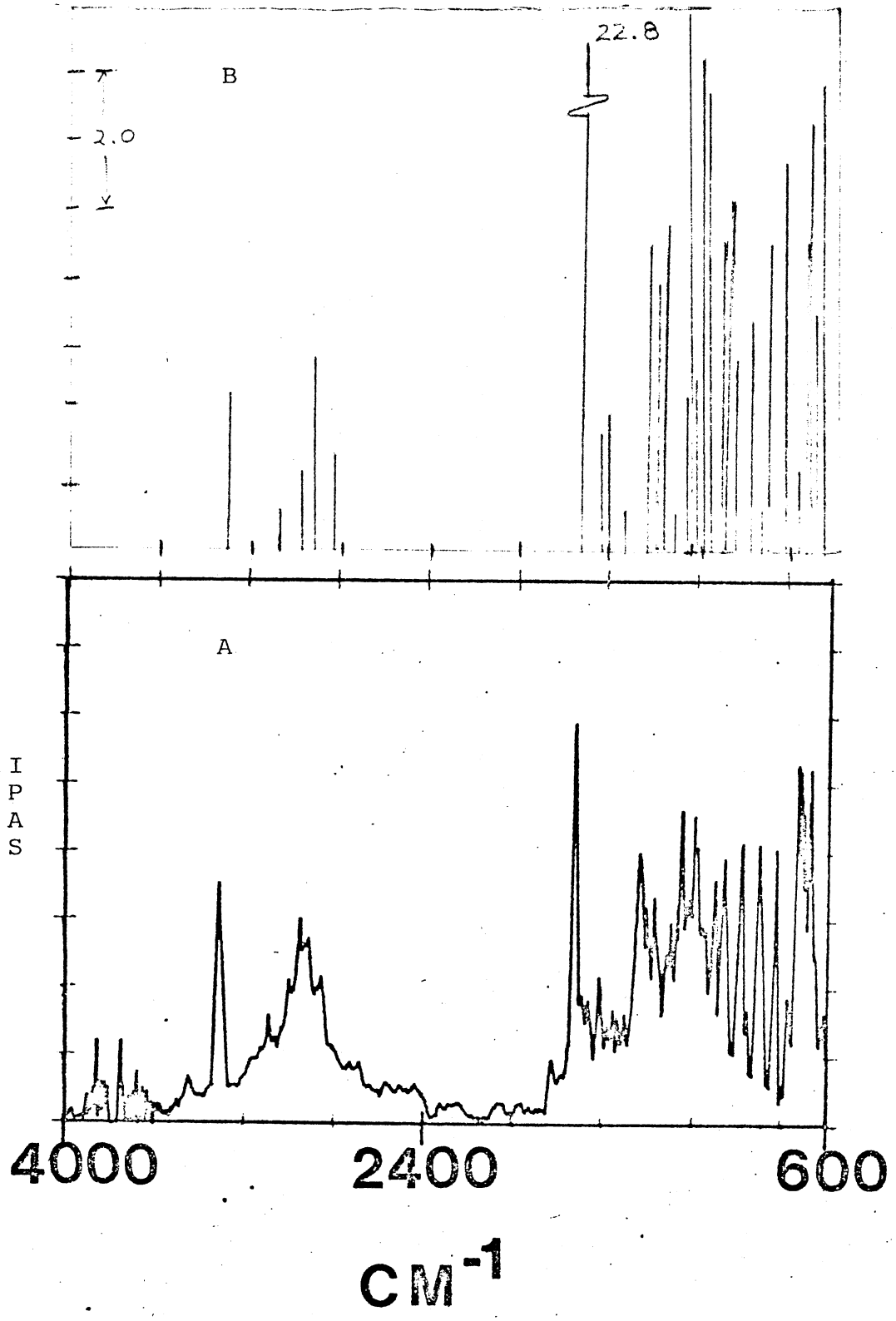

Figure 7. (A) 800 Scans of 7 mg of Protoporphyrin IX Dimethyl Ester at 8 cm^{-1} Resolution. Grade 1 Purity from Sigma Chemical Co. (B) Absorance Result for Protoporphyrin IX Dimethyl Ester.

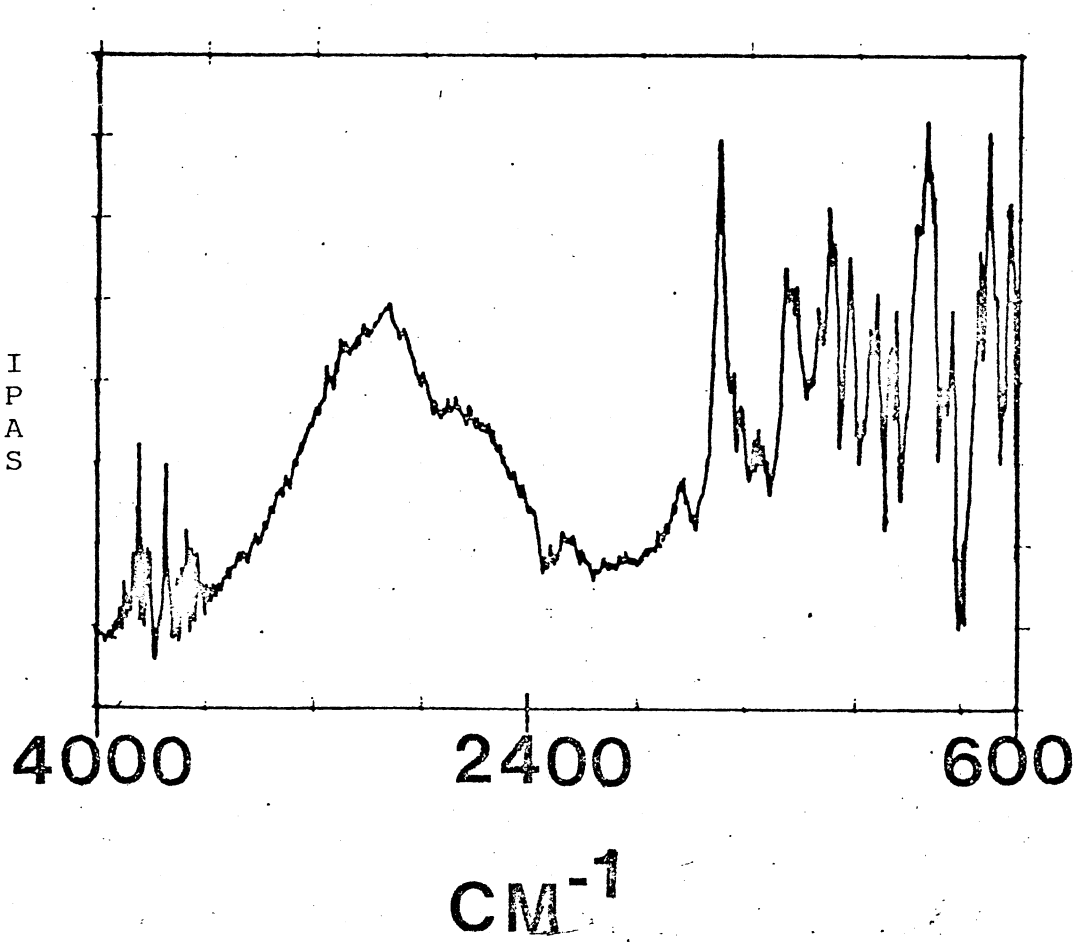

Figure 8. 800 Scans of 14 mg of Hemin-Bovine at 8 cm^{-1} Resolution. Grade 1 Purity from Sigma Chemical Co.

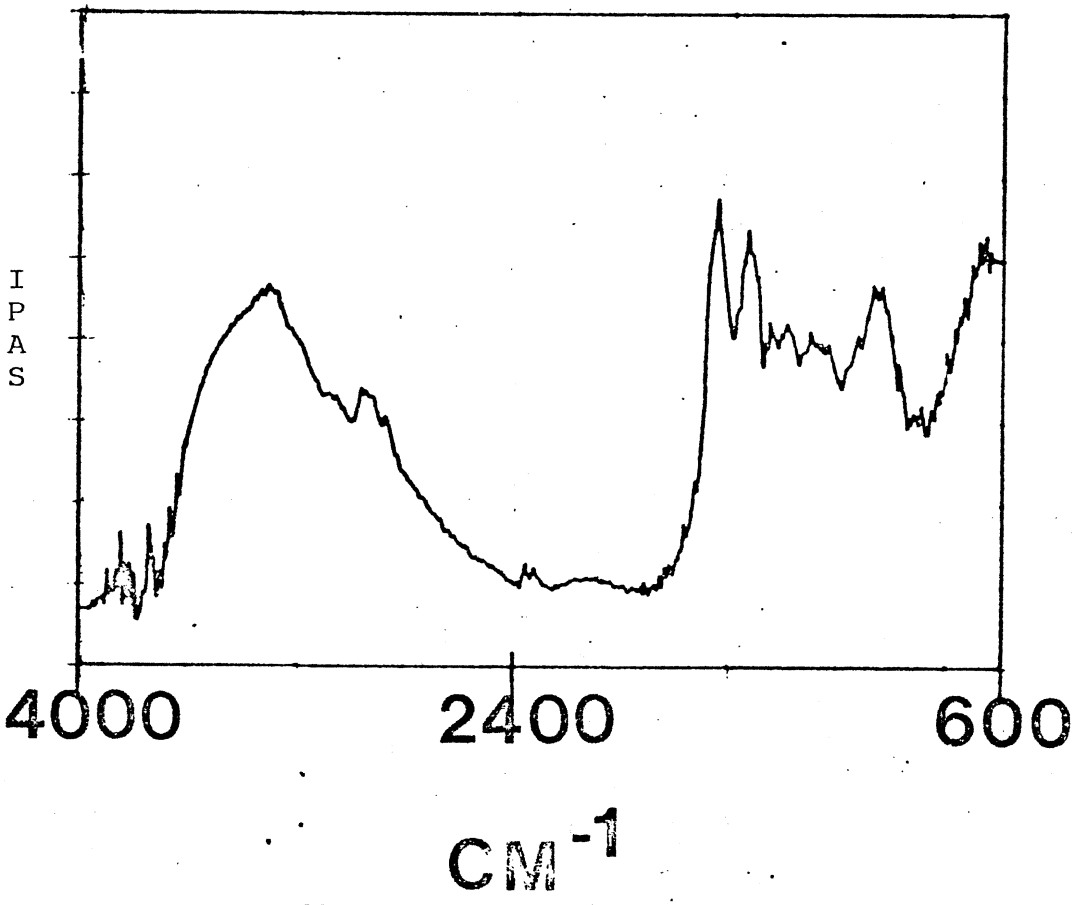

Figure 9. 800 Scans of 1 mg Hemoglobin at 8 cm^{-1} Resolution. Hemoglobin from Beef Blood Obtained from Sigma Chemical Co.

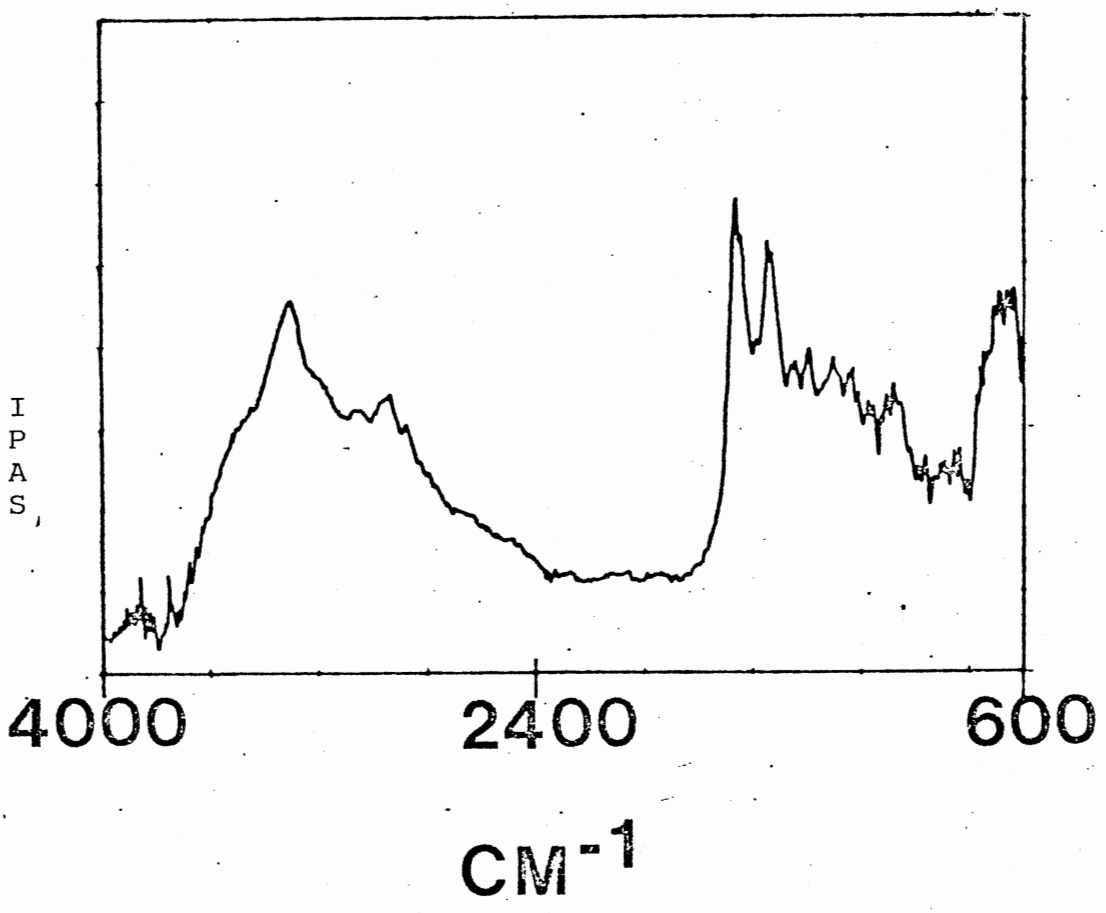

Figure 10. 200 Scans of 0.5 mg of Horseradish-peroxidase at Resolution 8 cm^{-1}. Type VI HRP Obtained from Sigma Chemical Co.

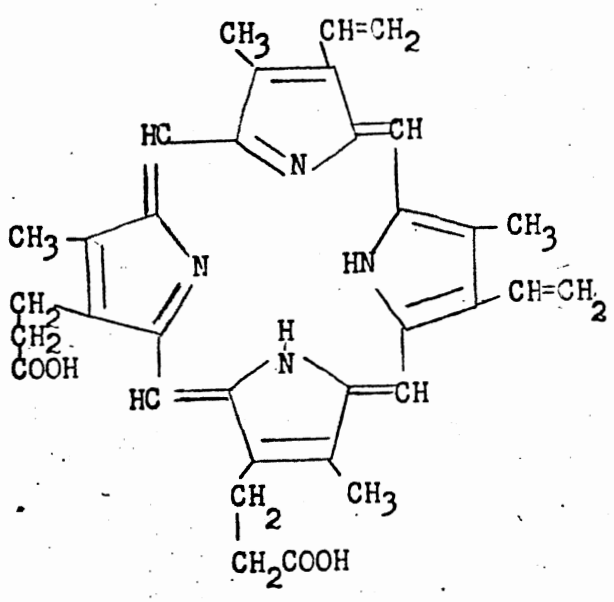

Figure 11. Protoprophyrin IX Dimethyl Ester

were not dissolved or pressed into a KBr pellet and were of total weight of ca: 1 mg.

Asbestos Fiber

The prominence of asbestos fiber as a contaminant of water supplies has prompted the development of several detection schemes for measuring low concentrations of this fiber. One of the more ingenious schemes is that proposed recently by Monchalin et al. (30). Using a CW HF laser, this group was able to measure a few points (corresponding to the laser lines) on the photoacoustic absorption spectrum of asbestos fiber in the 3400 cm^{-1} to 3800 cm^{-1}

region. They assigned the location for the two hydroxyl groups and showed that these absorptions were polarized. The suggestion was made that a photoacoustic detection scheme could be arranged using this anisotropic absorption as a distinguishing feature for the asbestos in the presence of other contaminants.

Because of this intriguing possibility, it was felt that a more detailed photoacoustic spectrum of asbestos fiber using the new technique of FTIR-PAS would be useful. The FTIR-PAS spectrum of asbestos fiber is shown in Figure 12. Several features of this spectrum are notable. Firstly, the sharp doublet at 3675 cm^{-1} due to the presence of non-hydrogen-bonded hydroxyls at two different locations within the crystallographic structure of asbestos (chrysotile) is apparent (30). The major peak has a maximum at 3692 ± 2 cm^{-1}, and the lesser peak is centered at about 3655 ± 5 cm^{-1}. These measurements are taken from an expansion of Figure 12 and agree, within experimental error, with those made by Monchalin et al.

Monchalin and coworkers (30) expected that the ratio of the intensities of the strong to weak bands in this doublet would be almost 3 to 1, based on analysis of the crystallographic structure of chrysotile. However, because they were using a line source for excitation (an HF laser), they were unable to clearly define the maximum PAS signal of the two components of this doublet. It is tempting to

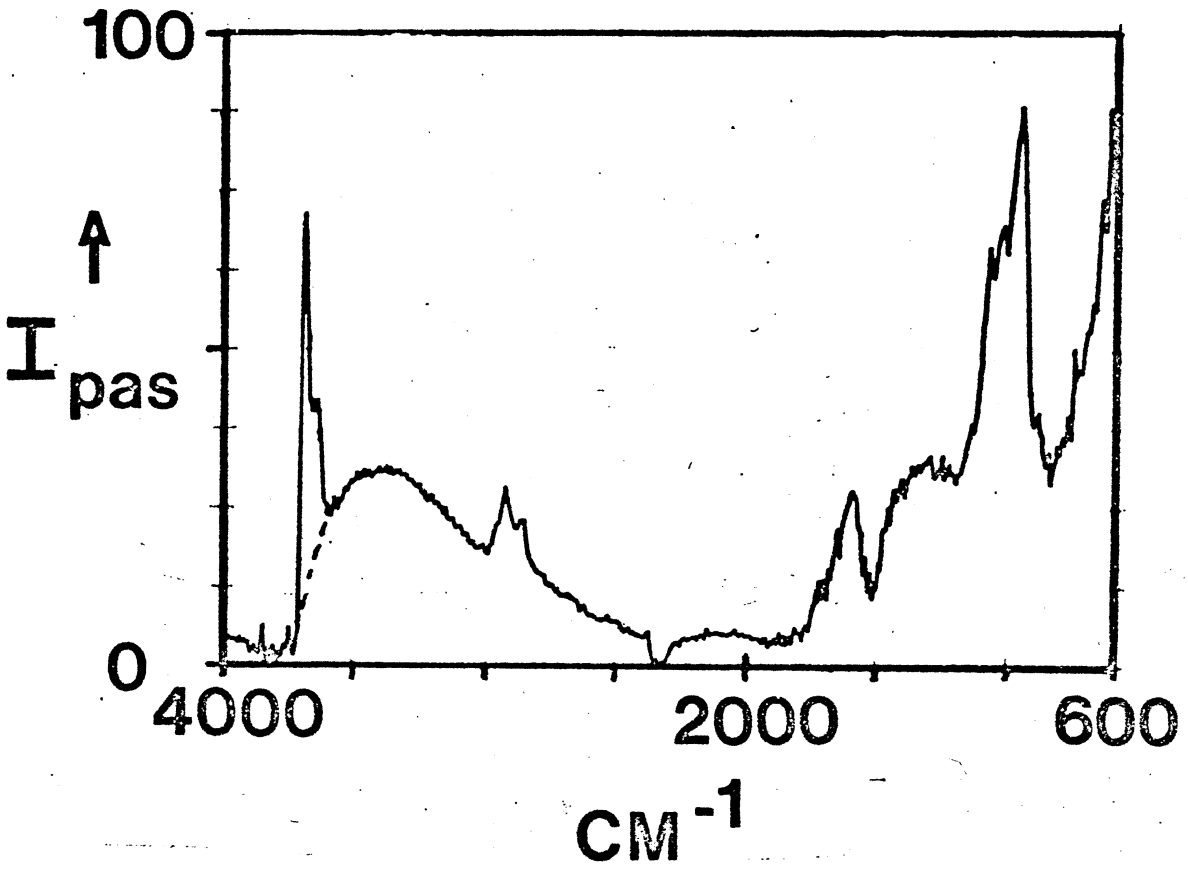

Figure 12. The Corrected FTIR-PAS Spectrum of Asbestos Fiber. 400 Scans at 8 cm^{-1} Resolution are Coadded.

extrapolate the absorption due to physisorbed water as has been done in Figure 12 (the dotted line) and then to obtain the net absorption strengths of the two components of the doublet (31). Analysis of an expanded spectrum in this manner does, indeed, yield a ratio of 3 to 1.

The final interesting feature of the spectrum in Figure 12 to be discussed here is the strong absorption at 945

cm^{-1}. It is readily apparent that this absorption is stronger than the absorption at 3692 cm^{-1} by about 25%. Coincidentally, the absorption is also centered at the emission wave length of the CO_2 laser. Since the CO_2 laser is more convenient to use in any detection scheme than an HF laser, and since the chrysotile PAS absorption at the CO_2 laser wavelength is stronger than at the HF laser wavelength, the CO_2 laser may well be the preferable excitation source for detection of asbestos fibers by photoacoustic spectroscopic methods.

Drugs

In the light of the great importance of drugs in society today, it was decided to devise experiments to see if PAS could give qualitative and quantitative information of known barbituates. FTIR-PAS spectra were obtained for a wide variety of biologically active drugs to determine if the technique would provide reproducible qualitative information. Spectra were obtained that gave qualitative results. The drugs were all related to the barbital family, which is a derivative of barbituric acid. (See Figures 13-17 for structures.) The samples tested spectroscopically by the PAS technique were Sodium Barbital (Fig. 18), Phenobarbital (Fig. 19), Amobarbital (Fig. 20), 5,5-diallyl Barbituric acid (Fig. 21), Hexobarbital (Fig. 22), Secobarbital (Fig. 23), and dl-Penobarbitol (Fig. 24).

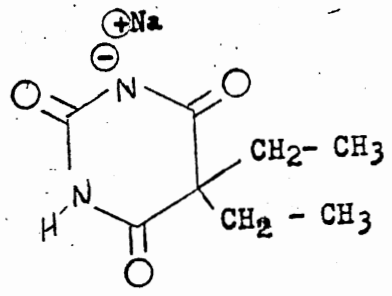

Figure 13. Sodium Barbitol
$C_8H_{11}N_2O_3Na$

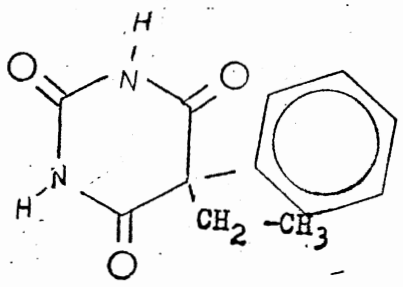

Figure 14. Pheonobarbital
$C_{12}H_{12}N_2O_3$
5-Ethyl-5-
Phyenyl-Bar-
bituric Acid

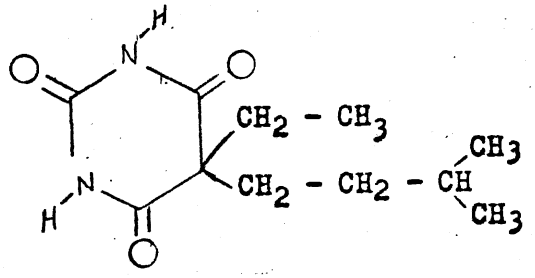

Figure 15. Amobarbital $C_{11}H_{18}N_2O_3$
5-Ethyl-5-(3Methyl Butyl) Barituric Acid.

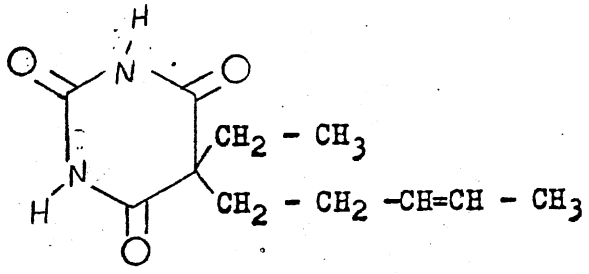

Figure 16. Pentobarbital $C_{11}H_{18}N_2O_3$
5-Ethyl-5(2-Pentyl)-Barbituric Acid.

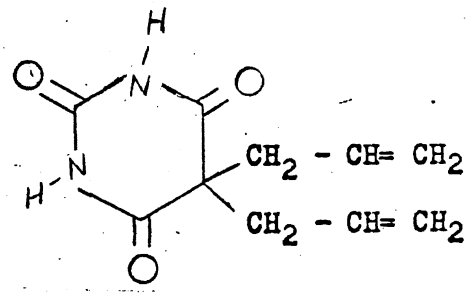

Figure 17. 5,5 Diallyl Barbituric Acid

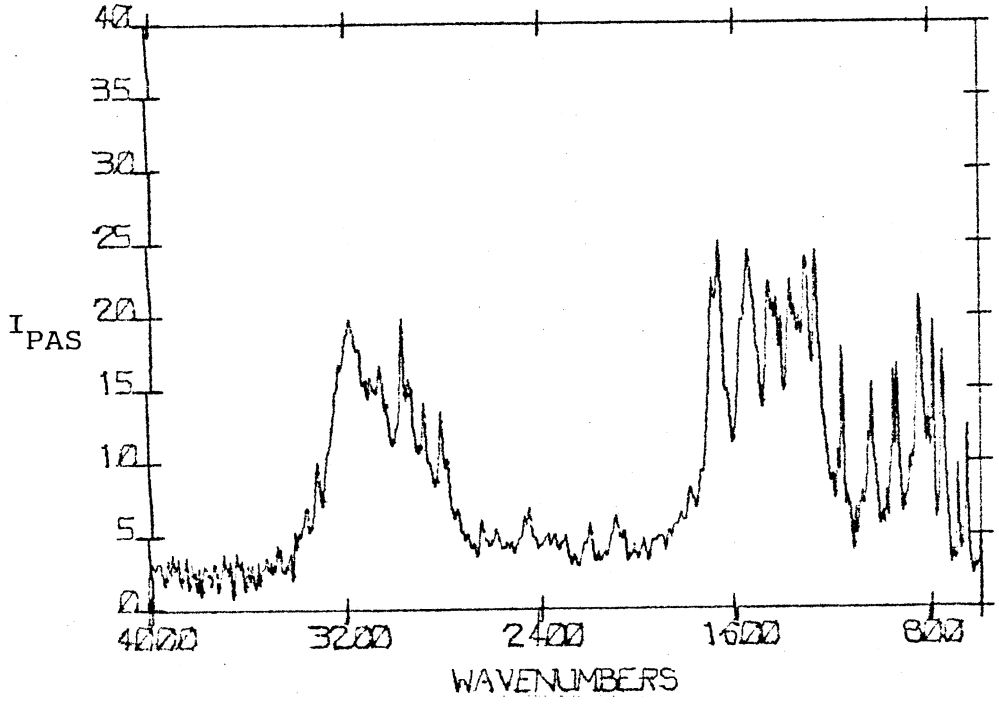

Figure 18. 800 Scans of Sodium Barbital at 8 cm^{-1} Resolution.

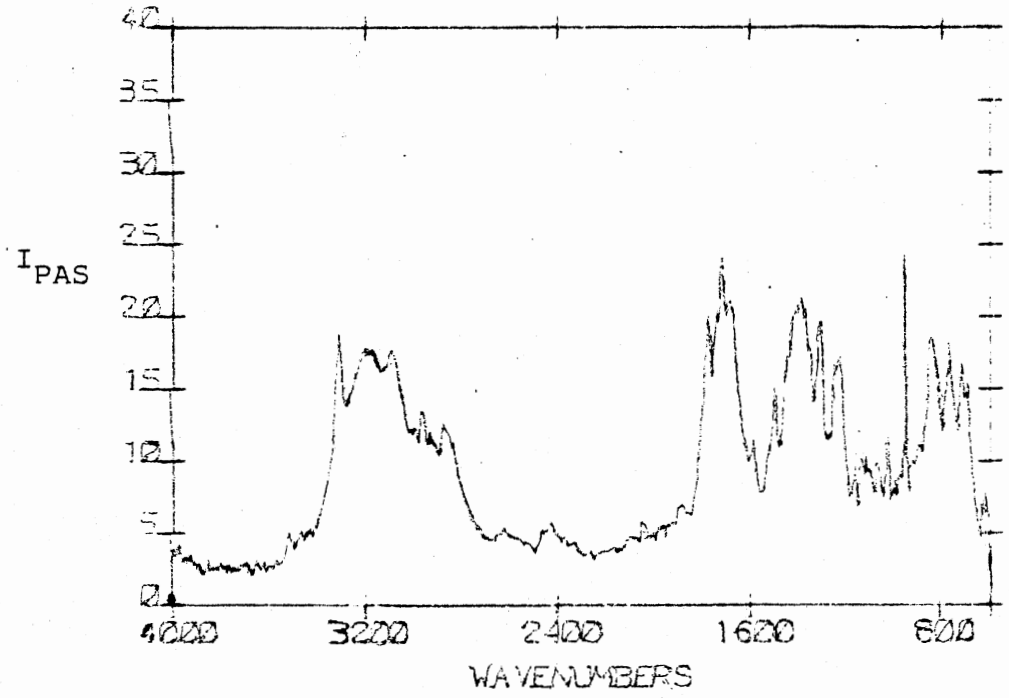

Figure 19. 800 Scans of Phenobarbital at 8 cm^{-1} Resolution.

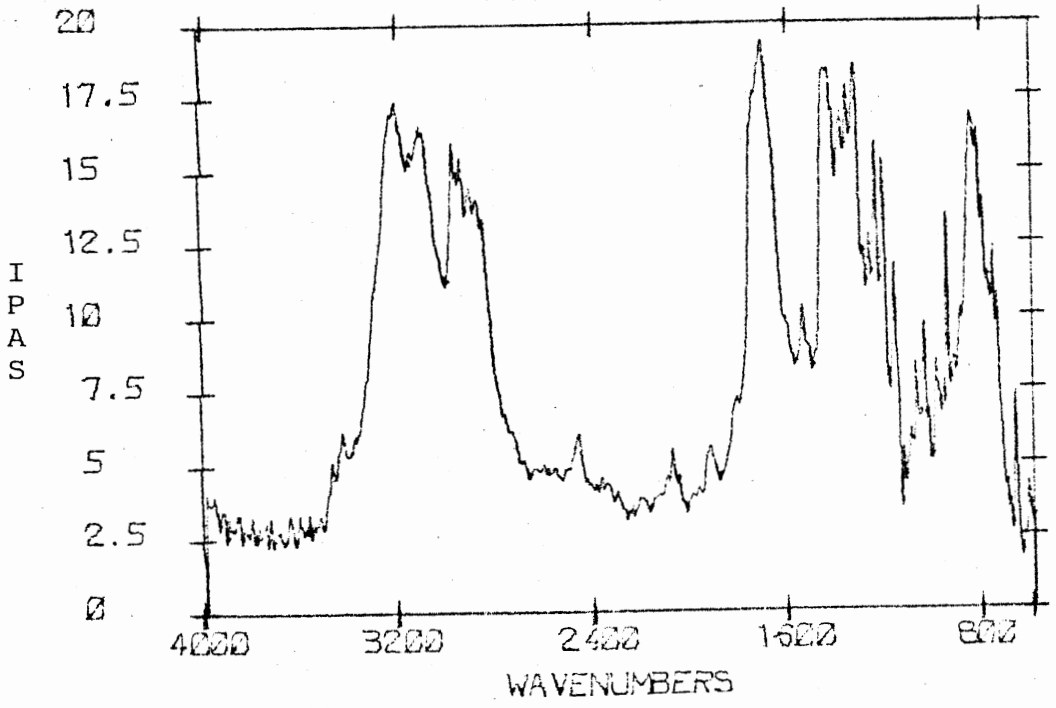

Figure 20. 800 Scans of Amobarbital at 8 cm^{-1} Resolution.

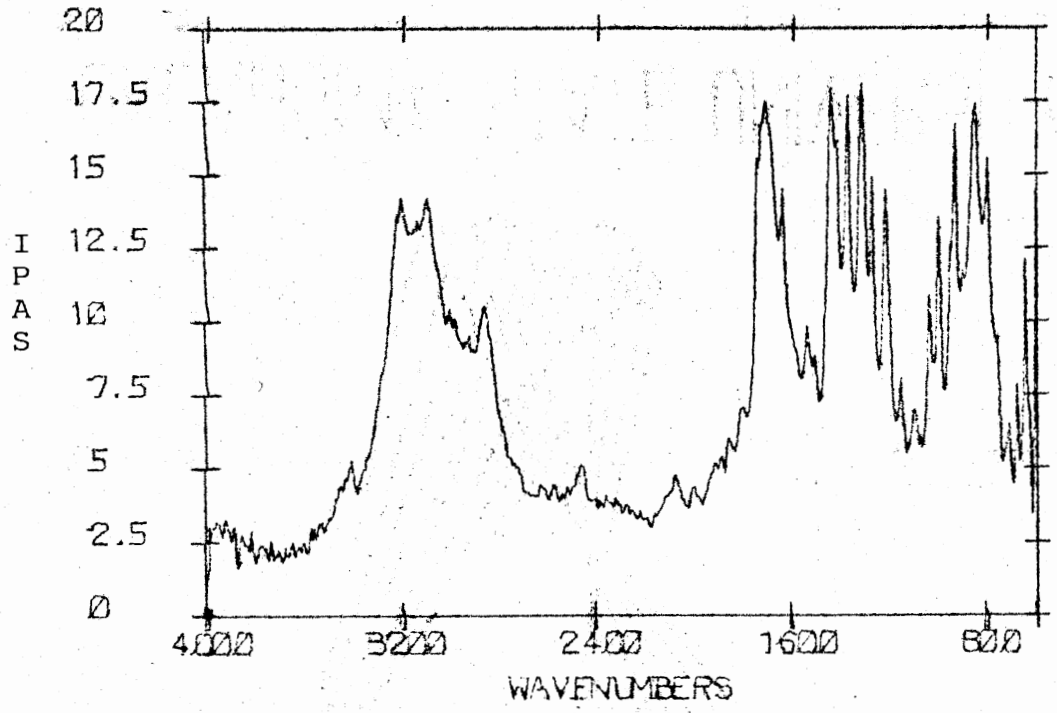

Figure 21. 800 Scans of 5,5 Diallyl-Barbituric Acid at 8 cm^{-1} Resolution.

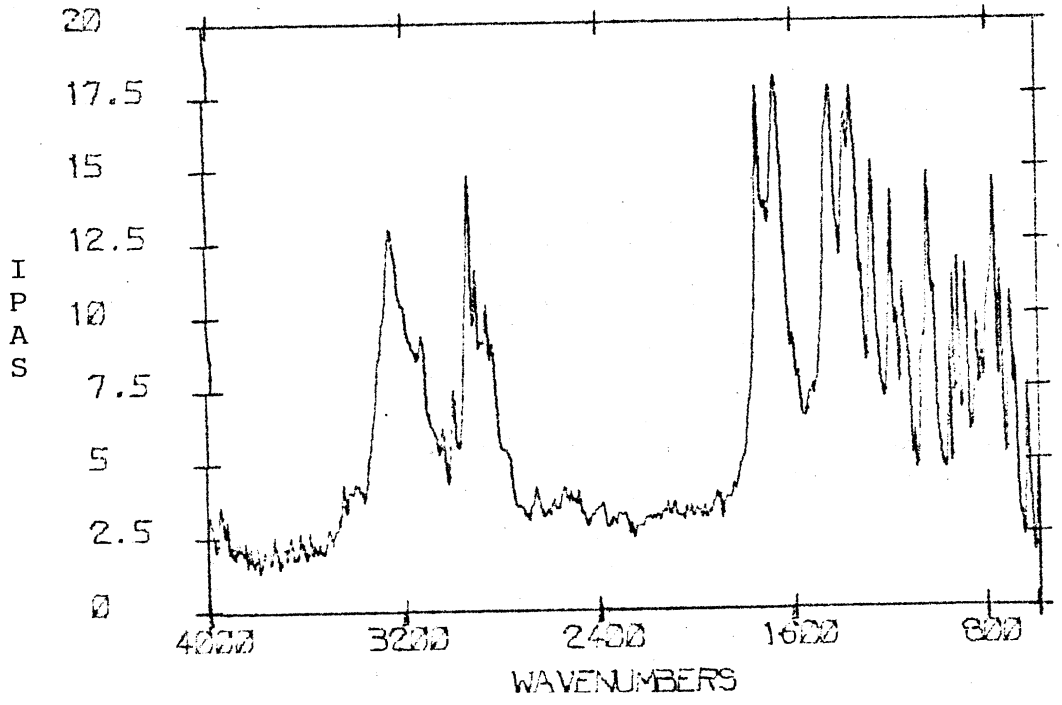

Figure 22. 800 Scans of Hexobarbital at 8 cm^{-1} Resolution.

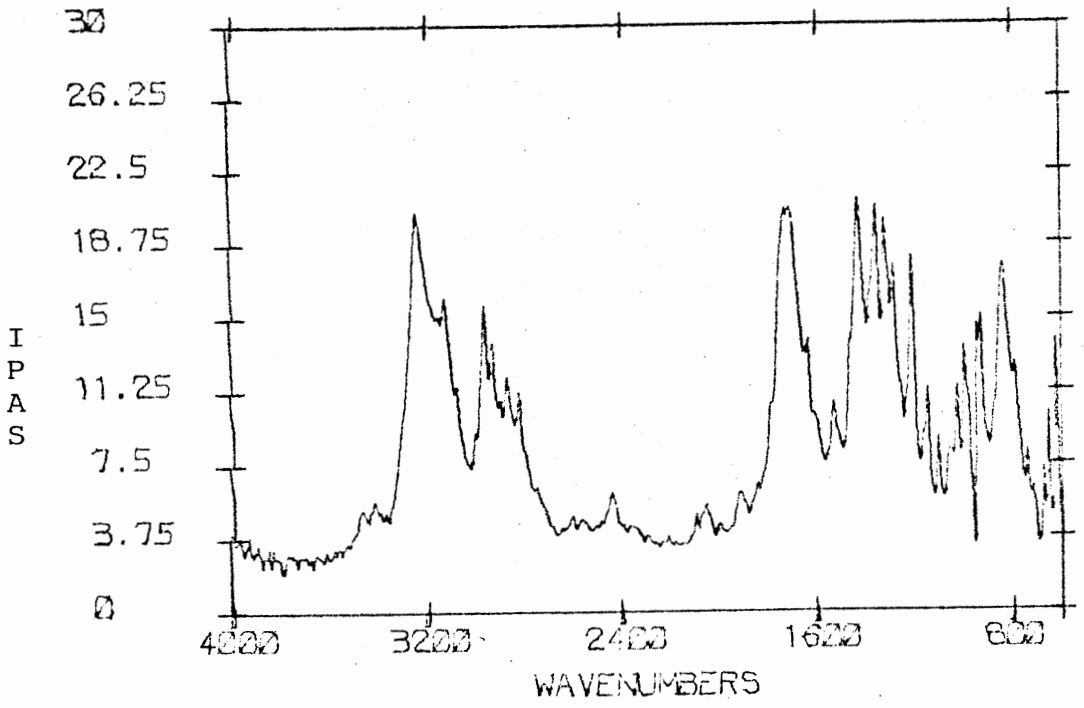

Figure 23. 800 Scans of Secobarbital at 8 cm^{-1} Resolution.

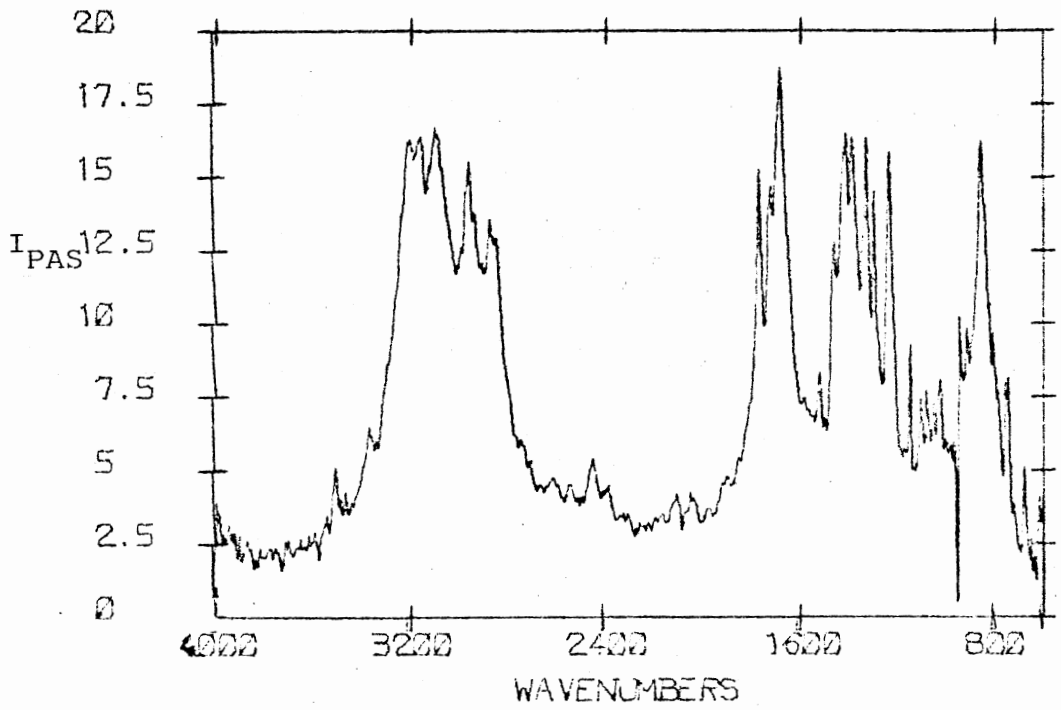

Figure 24. 800 Scans of dl-Pentobarbital at 8 cm^{-1} Resolution.

Each spectrum gives a characteristic grouping of frequencies around 3200 cm^{-1} and from 1800 cm^{-1} down to 600 cm^{-1}. Qualitatively each spectrum can be differentiated from any of the other spectra of the different drugs. Therefore, this technique could give useful qualitative information. The structure of the barbital backbone is shown in Figure 25. Differences between the molecules can

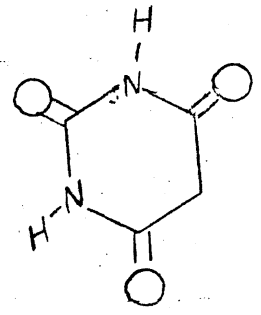

Figure 25. Barbital back-bone $C_6H_4N_2O_3$

be attributed to different substituents at the 5 position of the barbital backbone. The prominent non-hydrogen-bonded N-H stretch ($\backsim$ 3400 cm^{-1}) for Phenobarbital can be attributed to the fact that the phenyl group at the 5 position hinders hydrogen bonding of the nitrogen at the 1 and 3 positions, whereas in the other barbitals hydrogen

bonding might be occurring. Thus, this sharp peak is absent. The peak around 2800 cm^{-1} in the barbitals denotes the presence of aliphatic C-H. This is especially prominent for Secobarbital and Hexobarbital. The peak located at 1700 cm^{-1} can be attributed to a carbonyl stretch, as would be expected, while the fingerprint region is reserved for the different fundamentals associated with each different molecule. Since each type of drug is similar, but gives different PAS spectra, it is possible to use this technique to obtain pertinent qualitative information on subtle differences of molecules.

It has been established that PAS is useful for deriving qualitative data. Could this technique also produce useful quantitative results as well? To answer this question an experiment was devised to measure the absorbance of the ν_2 stretch of $K^{15}NO_3$ relative to the ν_2 stretch of $K^{14}NO_3$ with respect to $\%K^{15}NO_3$. It was hoped that the FTIR-PAS signal strength would be correlated with the percent by weight concentration of the $K^{15}NO_3$.

Quantitative Results

In the attempt to determine if the FTIR-PAS signal strength was correlated with the percent by weight concentration of the sample, the spectra of a set of mixtures of $K^{15}NO_3$ and $K^{14}NO_3$ were made. The $K^{15}NO_3$ was obtained with sincere thanks from J. P. Devlin who purchased

it from Stohler Isotope Chemical Company. Baker Chemical Company provided the $K^{14}NO_3$. Both chemicals were 99% isotopically pure. A set of mixtures of the two salts were carefully weighed. They were then ground with an agate mortar and pestle to increase the sample surface area and to insure sample homogeneity. In practice, the FTIR-PAS signal strength is dependent upon the particulate size. However, because these experiments relied on the measurement of relative absorption peak heights of the two salts, (Table I Appendix), the absolute signal magnitude was not an important consideration, provided the samples were homogeneous. Consequently, the salt mixtures were not sized.

Figure 26 shows the unsmoothed, unretouched FTIR-PAS spectra of pure KNO_3 and a mixture of the two KNO_3 salts. While the compressed spectra look quite similar, the inset, which shows an expansion of the spectrum in the vicinity of the ν_2 absorption at 825 cm^{-1}, clearly shows the isotopic shift expected and the presence of the two components in the 50:50 mixture. The bottom spectra are of the pure $K^{14}NO_3$, while the top are spectra of a 50:50 mixture of $K^{15}NO_3$ and $K^{14}NO_3$. One other notable feature shown in the insert of Figure 26 concerns the relative peak heights apparent for the 50:50 mixture. The absorption band centered at 825 cm^{-1} for the ^{14}N salt tails off to about 20% of the maximum intensity at 800 cm^{-1} where the ν_2 absorption of the ^{15}N

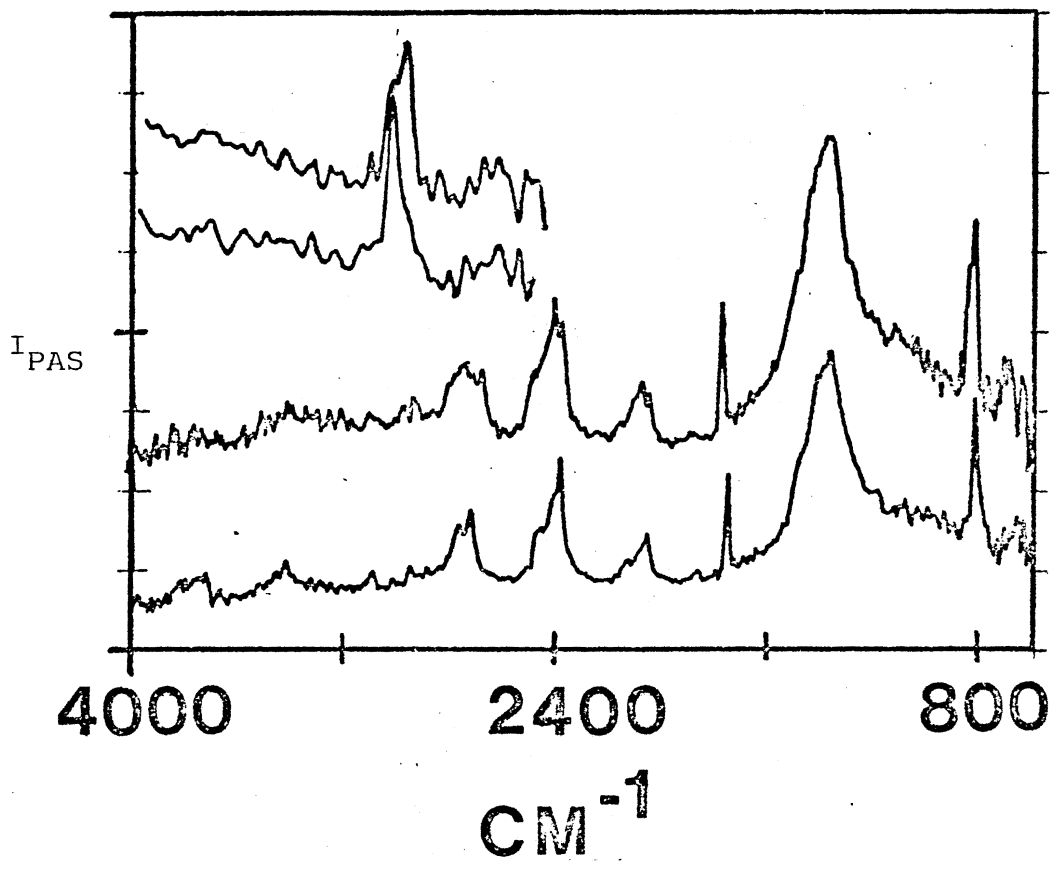

Figure 26. The FTIR-PAS Spectra of $K^{14}NO_3$ (Lower Spectra) and a 50:50 Mixture of $K^{14}NO_3$ and $K^{15}NO_3$ (Upper Spectra). The inlet Shows an Enlargement of the Two Spectra in the Vicinity of the 825 cm^{-1} Absorption. 1000 Scans at 8 cm^{-1} Resolution Were Coadded for Each Spectrum.

salt appears. Thus, the ^{15}N absorption appears to be more intense in the 50:50 mixture, but only by virtue of being situated on the shoulder of the ^{14}N.

To obtain an estimate of the quantitative dependence of the FTIR-PAS signal strength on the relative percentage of each salt, the $_2$ absorption feature at 825 cm^{-1} was analyzed. The intensity of this absorption feature (generally consisting of two bands, due to the two different salts) at 800 cm^{-1} was ratioed to the sum of the intensitites at 825 cm^{-1} and 800 cm^{-1}. In this manner, a relative signal strength for the ^{15}N salt absorption was obtained for each mixture. The reliability of this approach was verified by measuring the FTIR-PAS spectra of the pure salts individually, adding the two spectra together in different percentages and analyzing this synthetic data in the same fashion as described above (Table II, Appendix).

Figure 27 is a graphical representation of the relative absorbance by $K^{15}NO_3$ as a function of the weight percentage of this salt in the mixture. A least squares fit of the data gives a straight line with a slope of .65 and a correlation coefficient of .98. This line intercepts the ordinate at .24. This is not to say that the $K^{14}NO_3$ was 25% $K^{15}NO_3$. Rather this intercept represents the relative height of the shoulder on the $K^{14}NO_3$ absorbance. For similar reasons, 100% $K^{15}NO_3$ registers as 90% purity. That is, there is a smaller but finite high frequency tailing of the $K^{15}NO_3$ absorption (32).

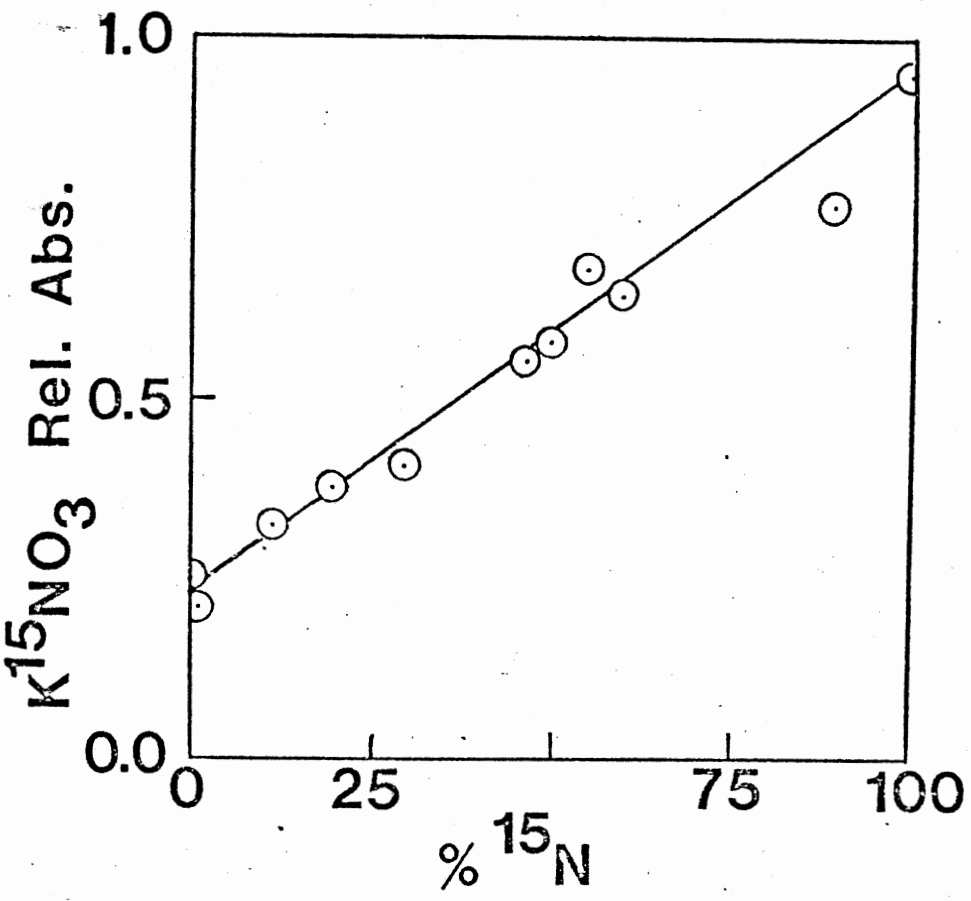

Figure 27. Relative Peak Intensity at 800 cm^{-1} Vs. 825 cm^{-1} Plotted Against % $K^{15}NO_3$. The Least Square Line Fits the Data With a Correlation Coefficient of 0.98.

Quality of Spectra

The final unanswered question deals with the factors affecting the quality of obtainable spectrum. To answer this question a set of experiments were developed to study the signal-to-noise ratios obtainable from each of several different cell designs and to study the effect of particle size on the spectra. For the sake of convenience the cell shown in Figure 4 will be called the "grease cell" (referring to the grease used as a sealant), and the cell in Figure 5 will be called the "minimum volume cell".

Figures 28 and 29 show a comparison of the two cells listed above. In the grease cell the microphone used was the General Electret (model 1962), which has a sensitivity of 10 mvolts/microbar. The preamplifier used for both cells was the Ithaco low-noise 40 dB preamplifier (model 143L). The microphone for the minimum volume cell was the Bruel Kjaer 1/2" foil electret (model 4175), which has a sensitivity five times that of the GRE microphone, or about 50 mvolts/microbar. The top spectrum is the 100% line of carbon black at 20 scans for the minimum volume cell. Notice that little, if any, improvement of signal-to-noise was obtained for the more sensitive cell despite the approximate doubling of the signal intensity (Fig. 30). The noise ratio was about 2% of the signal at best. However, the elimination of room noise has resulted in a 1% noise ratio compared to the signal. However, experiments

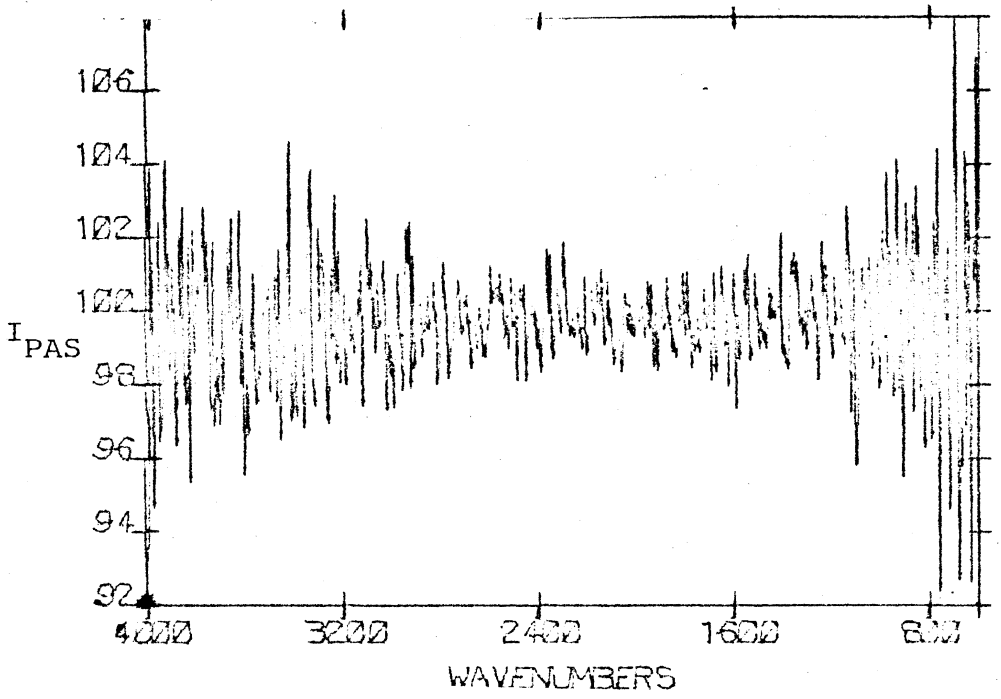

Figure 28. 100% Line for Greased Cell with Lower Sensitive Microphone.

conducted on low absorbing materials showed that the number of scans were halved to obtain the same noise ratio. This preliminary conclusion is based on the difference in number of scans used to obtain Sodium barbital (Fig. 18) with the greased cell and Ithaco microphone, compared to that obtained with the minimum volume cell and B & K microphone (Fig. 31). In the first case 800 scans were needed, and a signal-to-noise ratio of about 33 was obtained. For the B & K microphone only 320 scans were required for about the same signal-to-noise ratio (Fig. 31).

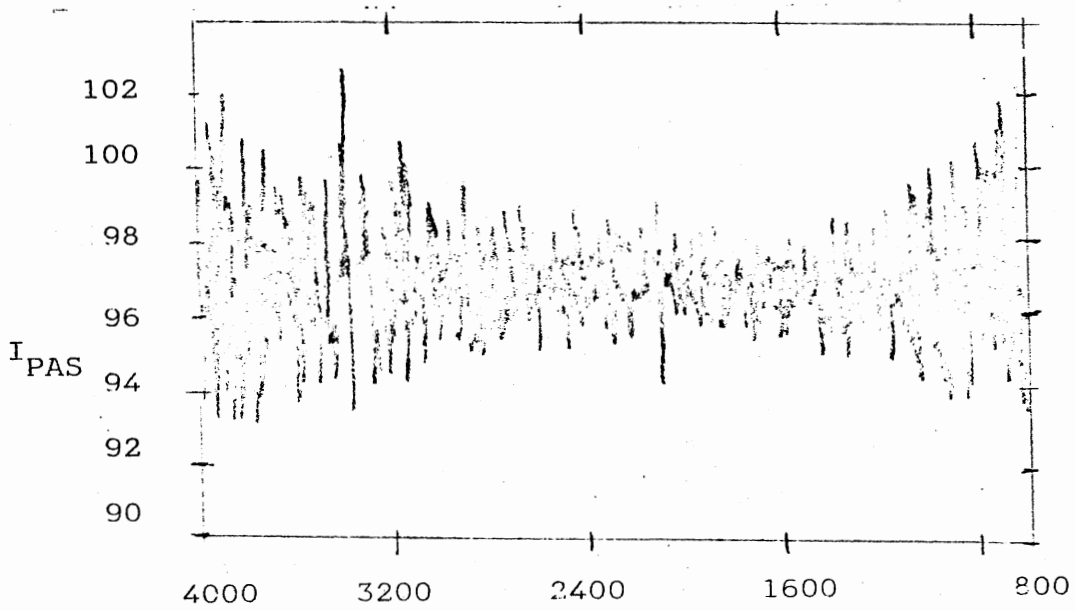

Figure 29. 100% Line for Minimum Volume Cell With Higher Sensitive Microphone.

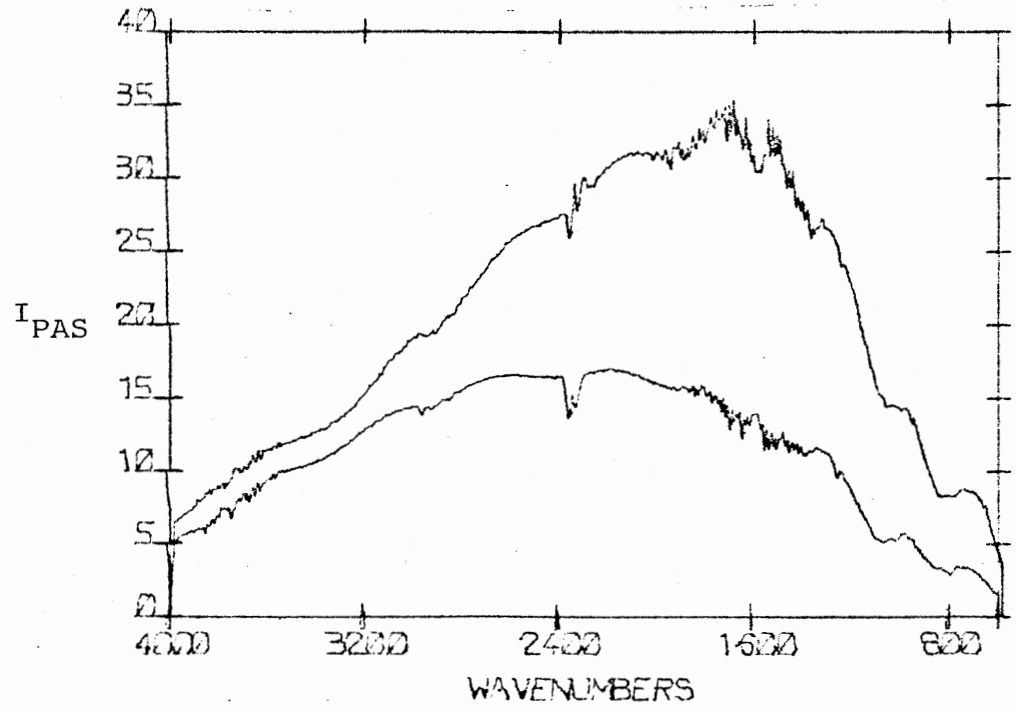

Figure 30. Single Beam Spectrum - 1000 Scans of Carbon Black at 8 cm^{-1} Resolution.

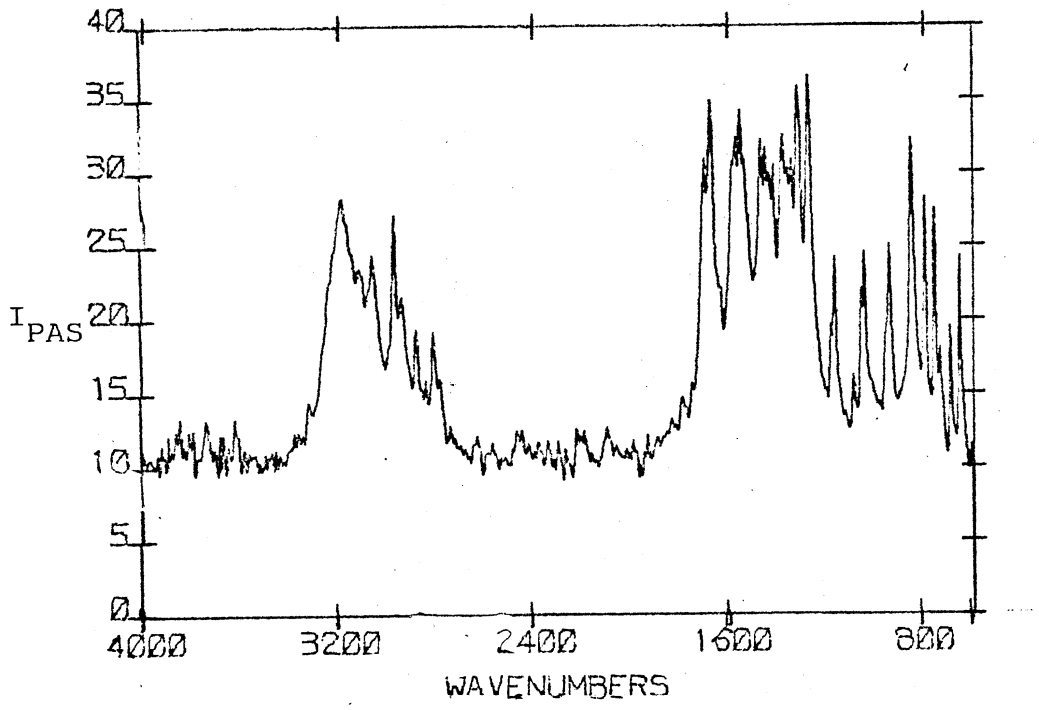

Figure 31. 320 Scans of Sodium Barbital on 8 cm^{-1} Resolution. Spectrum Obtained with Higher Sensivity Microphone.

However, the results are far from conclusive, and more work is being done in this area.

A second parameter affecting the quality of spectra is the effect of particle size of the sample upon peak height. The first theoretical treatment of this subject is attributed to Lord Rayleigh who concluded that the amount of scattering was inversely proportional to the fourth power of the incident wavelength, and is directly proportional to the cube of the particle diameter size (33). Lower scattering at lower frequencies and lower particle sizes would be expected. This has been noted in the study of surface hydroxyls in which the quality of the spectrum obtainable with deuterated samples was superior to the quality of the hydrogenated samples. The OD peak is around 2700 cm^{-1}, while the DH peak is around 3600 cm^{-1}. Since the OD peak is at lower frequencies, the signal intensity would be expected to be greater, because the scattering would be less.

A study of the amount of scattering produced by a collection of particles was made by Duyckaerts (34). He assumed that particles of density "ρ" and diameter "d" were dispersed randomly in a disk of cross-sectional area "S", mass "M" and length "l". He also assumed that the disk was arranged in "Ω" layers, and that the incident light interacts with each particle only one time. He concluded that

$$I / I_o = [\ (1 - K) + K\theta\ ]^n$$

where "K" represents the geometrical fraction of the surface where the light is focused, and θ is the transmission of one particle. From Beer's law the following equation is obtained.

$$\theta = \exp [\ -\alpha d\ ]$$

α is the true extinction coefficient of the material. From the above equation the following equation is obtained.

$$\log I_o / I = A = -n \log [\ (1 - K) + K\theta\ ]$$

Determining "n" from ρ, d, S, M, K, Duyckaerts obtained

$$A_{\lim \alpha d \to 0} = M\alpha/S\rho\ 2.3$$

He plotted 2.3 A S ρ /M against d and showed that the maximum transmission was obtained when the particle size was less than the wavelength of the incident light.

To obtain an estimate of the importance of this phenomena in FTIR-PAS measurements, a study centered on using Silica dust of known particle sizes (Silica dust was obtained from Fluid Power Research at OSU). The samples were 0-5 microns and 55-60 microns (Fig. 32), 10-15 microns, 20-25 microns, 30-35 microns and 50-60 microns (Fig. 33). The peak of interest was the peak around 1100 cm^{-1}, which is due to the Si-O stretch. A comparison of different particle sizes with respect to photoacoustic spectroscopy was expected to confirm Duyckaerts' findings. The peak height was analyzed in the usual fashion of relative peak intensity. For example (Table III, Appendix), the peak

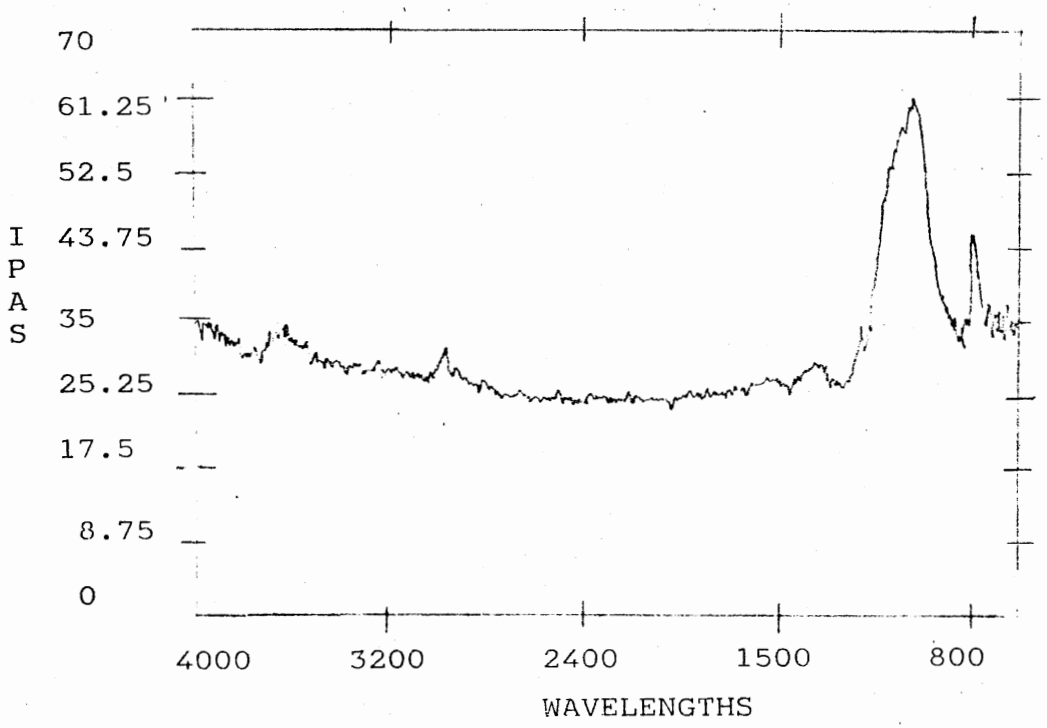

Figure 32. 1000 Scans of Silica Dust at 8 cm^{-1} Resolution. The Particle Size was 0-5 Microns.

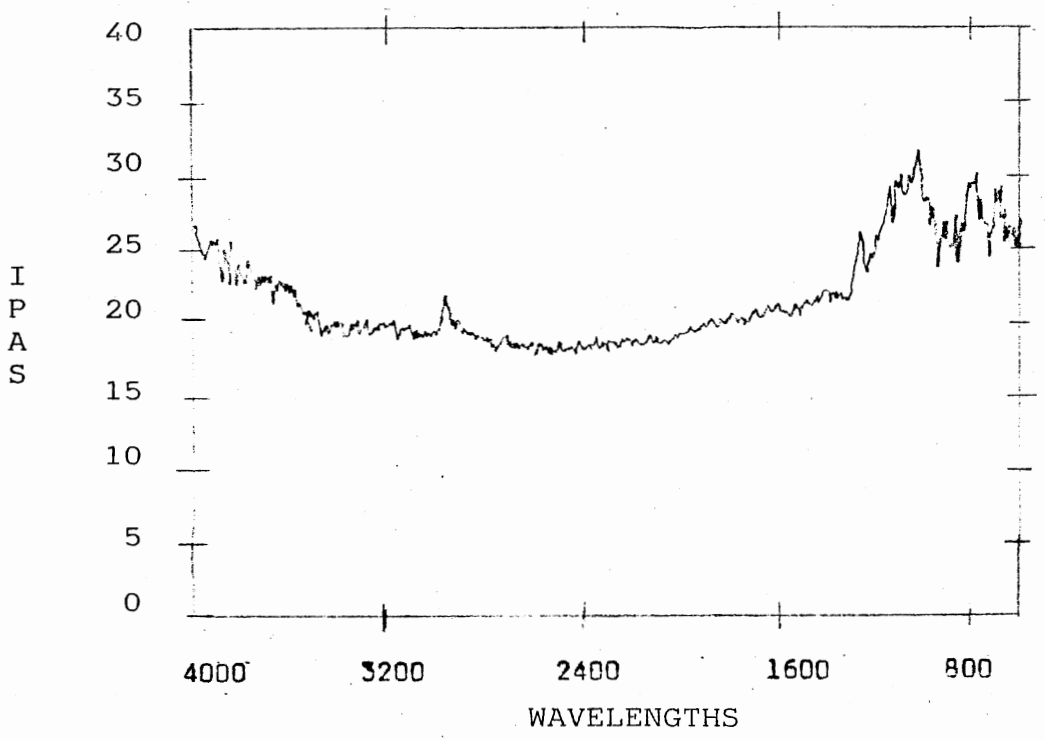

Figure 33. 1000 Scans of Silica Dust at 8 cm^{-1} Resolution. The Particle Size was 55-60 Microns.

height for the 0-5 micron Silica dust was found to be 74. The baseline signal at around 2500 cm^{-1} was 14. Therefore, the relative peak height of the signal at 1100 cm^{-1} is (74-14)/14, or 4.29. The reason for using this relative scale is to eliminate any differences from samples due to scattering or different depth profiles. The particle size that is associated with the wavelength of light at 1100 cm^{-1} is approximately 10 microns. As the particle sizes approached this wavelength the band intensity relative to the background was enhanced considerably (Fig. 34). Thus,

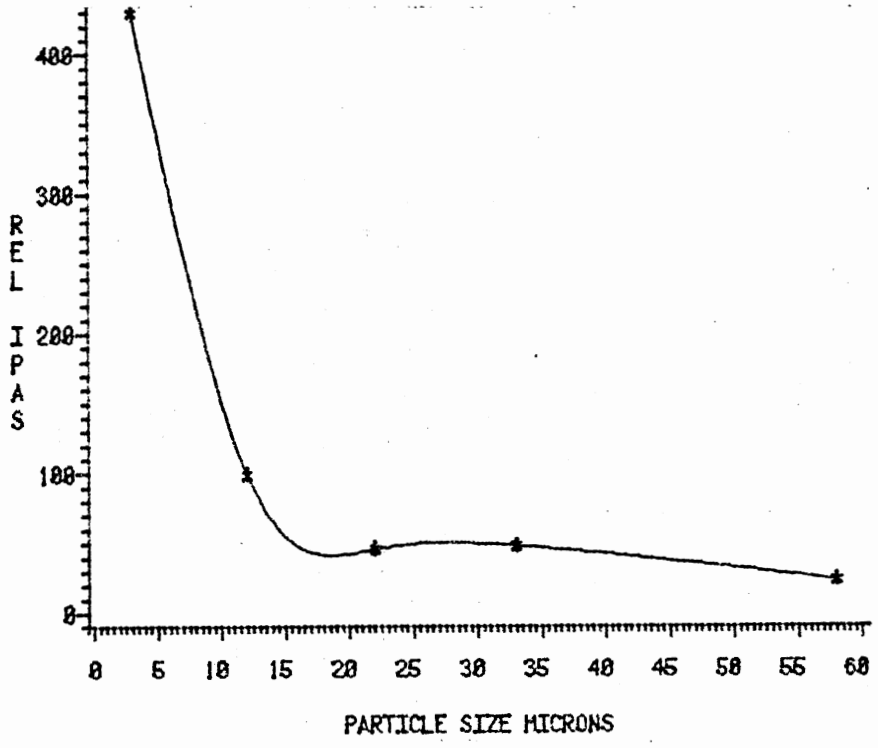

Figure 34. Plot of Particle Size of Silica Dust Vs. I_{PAS} at 100 cm^{-1}.

the same effects for transmission spectroscopy with respect to solid particle size applies to photoacoustic spectroscopy as well. Since Duyckaerts concluded that the resolution should also be affected by particle size, more work needs to be done to determine if this holds for photoacoustic spectroscopy as well. An assumption used by Duyckaerts was that the particles were embedded in a media of equal refraction index. Since this is clearly not the case in gas-solid interfaces, more work also needs to be done to determine the relationship between signal enhancement and the difference between the refractive indices of the solid and gas interface.

Conclusion

Through the above experiments it has been determined that the FTIR-PAS signal of condensed media provides insightful qualitative information on three different types of solids - biological materials, asbestos fibers and biologically active drugs. It has been shown that FTIR-PAS gives quantitative information for samples that were nearly identical. However, whether or not this technique can be used to obtain quantitative information on mixtures of different absorption coefficients has not been determined. More research is needed in this area to determine if quantitative information can be obtained on various types of media. The photoacoustic effect has been shown to depend

upon the modulation frequency utilized. Therefore, care must be taken with sample preparation. Because the FTIR-PAS spectrum arises from sampling depths which vary with the infrared modulation frequency, the previous samples were considered homogeneous. If, however, the media were not homogeneous, this factor must be taken into account. Certain external parameters were shown to play an important role in determining the quality of spectra obtainable. The cell design as well as the microphone used were closely linked to the number of scans necessary to obtain enhanced signal-to-noise ratios. The particle size of the condensed media was also shown to affect the signal intensity of the photoacoustic effect. The enhancement of signal at lower frequencies is believed to be due to an increased scattering of the sample. However, experiments have not been conducted to determine how the resolution of the FTIR-PAS spectrum is changed by particle size and the dependence upon the refractive index of the media used.

BIBLIOGRAPHY

1. Bell, A. G., Am. J. Sci., 20, 305 (1880).

2. Bell, A. G., Philos. Mag., 11, (5 510 (1881).

3. Tyndall, J., Proc. T. Soc. Land., 31, 307 (1881).

4. Roentgen, W. C., Philos. Mag., 11, (5 308 (1881).

5. Viengerov, M. L., Dokl. Akad. Nauk. SSSR, 19, 687 (1938).

6. Pfund, A. H., Science, 90, 326 (1939).

7. Luft, K. F., Z. Tech. Phys., 24, 97 (1943).

8. Viengerov, M. L., Dokl. Akad. Nauk. SSSR, 46, 182 (1945).

9. Gorelik, G., Dokl. Akad. Nauk, SSSR, 54, 779 (1946).

10. Slobodskaya, P. V., Izv. Akad. Nauk. SSSR, Ser. Fiz., 12, 656 (1948).

11. Rosencwaig, A., Photoacoustics and Photoacoustic Spectroscopy, Chapter 9, John Wiley and Sons, New York, New York, 1980.

12. Harshbarger, W. R., and Robins, M. B., Acc. Chem. Res., 6, 329 (1973).

13. Harshbarger, W. R., and Robins, M. B., Chem. Phys. Lett., 21, 462 (1973).

14. Kaya, K., Harshbarger, W. R., and Robins, M. B., J. Chem. Phys., 60, 4231 (1974).

15. Kaya, K., Chatelain, C. L., Robins, M. B., and Keubler, N., J. Am. Chem. Soc., 97, 2153 (1975).

16. Robins, M. B., and Keubler, N. A., J. Am. Chem. Soc., 97, 4822 (1975).

17. Rosencwaig. A., Photoacoustics and Photoascoustic Spectroscopy, Chapter 9, John Wiley and Sons, New

York, New York, 1980.

18. Parker, J. G., Appl. Opt., 12, 64 (1973).

19. Rosencwaig. A., and Gersho, A., Science, 190, 556 (1975).

20. Rosencwaig, A., and Gersho, A., J. Appl. Phys., 47, 64 (1976).

21. Bennett, H. S., and Forman, R.A., Appl. Opt., 16, 101 (1976).

22. Aamodt, L.C., Murphy, G. C., and Parker, J. G., J. Appl. Phys., 48, 927 (1977).

23. Wetsel, G. C., Fr., and McDonald, F.A., Appl. Phys. Lett., 30, 252 (1977).

24. Rosencwaig, A., Photoacoustics and Photoacoustics Spectroscopy, John Wiley and Sons, New York, New York, 1980, p. 187.

25. Farrow, M. M., Brunham, R. K., and Eyring, E. M., Appl. Phys. Lett., 33, 735 (1978).

26. Rockely, M. G., Chem. Phys. Lett., 68(2-3), 455-6 (1979).

27. Rosencwaig, A., Photoacoustics and Photoacoustic Spectroscopy, in Chemical Analysis: A Series of
28. Monographs on Analytical Chemistry and Its Application, Vol. 57, P. J. Elving and J. D. Winefordner (Eds.), I. M. Kolthoff (Ed. Emeritus).

29. Spectrum No. 8725K, Sadtler Research Lab, Catalog, 1967.

30. Monchalin, J. P., Gagne, J. L., and Bertrand, L., Appl. Phys. Lett., 35, 360 (1977).

31. Gadsden, J. Parker, and Smith, W. L., Atm. Env., 4, 667 (1970).

32. Rockley, Mark G., Davis, D. M., and Richardson, H. H., Jr., Science, 210 (4472), 918-20 (1980).

33. Hair, Michael, Infrared Spectroscopy in Surface Chemistry, Marcel Dakker Inc., New York, 1967, pp. 59-61.

34. Duyckaerts, G., Analysist, 84, 201 (1959).

APPENDIXES

TABLE I

DETERMINATION OF RELATIVE I_{PAS} OF $K^{15}NO_3$

$K^{14}NO_3$ peak height (cm)	$K^{15}NO_3$ peak height (cm)	rel. I_{PAS} $K^{15}NO_3$ (exp.)
7.35	2.50	.25
8.00	4.85	.38
5.10	6.25	.55
4.95	3.50	.41
4.90	6.85	.58
7.45	3.45	.32
5.90	10.5	.64
11.3	3.00	.21
2.20	4.60	.68
3.80	7.00	.65
2.70	9.25	.77

TABLE II

$\%K^{15}NO_3$ VS. RELATIVE I_{PAS} OF $K^{15}NO_3$

rel. I_{PAS} $K^{15}NO_3$ (exp.)	rel. I_{PAS} $K^{15}NO_3$ (calc.)	% $K^{15}NO_3$
.25	.27	0.000
.38	.38	.196
.55	.58	.469
.41	.47	.298
.58	.59	.500
.32	.33	.114
.64	.64	.600
.21	.24	.001
.68	.61	.550
.95	.95	1.000
.65	.71	.777
.77	.79	.895

slope .650 (exp.) slope .640 (calc.)

corr. .977 (exp.) corr. .992 (calc.)

TABLE III

I_{PAS} OF SiO_2 PARTICLE SIZE IN MICRONS

SiO_2 peak height/baseline	rel. I_{PAS} SiO_2 (exp.)	particle size (micrometers)
41.3/33.5	.23	55-60
56.8/28.6	.99	10-15
33.0/22.3	.48	30-35
74.0/14.0	4.29	0-5
52.0/35.5	.46	20-25

VITA

Hugh Hill Richardson, Jr.

Candidate for the Degree of

Master of Science

Thesis: FOURIER TRANSFORMED INFRARED PHOTOACOUSTIC SPECTROSCOPY OF SOLIDS

Major Field: Chemistry

Biographical:

Personal Data: Born in Ft. Wayne, Indiana, November 19, 1954, the son of Hugh and Leslie Richardson. Married August 11, 1973 to Linda M. Cochren. One son born January 28, 1977.

Education: Graduated from New Haven High School, New Haven, Indiana, May, 1973; received Bachelor of Science degree in Biomedical Chemistry from Oral Roberts University, Tulsa, Oklahoma, May, 1979; completed requirements for Master of Science degree at Oklahoma State University in May, 1982.

Professional Experience: Member of Beta Beta Beta Biological Honor Society; member of Phi Lambda Upsilon Chemical Honor Society; graduate teaching assistant, Oklahoma State University, 1979-1981; research assistant, Oklahoma State University, 1981.